Journal of Solid Mechanics Vol. 13, No. 2 (2021) pp. 164-185
DOI: 10.22034/jsm.2020.1895313.1561

Size-Dependent Vibration Problem of Two Vertically-Aligned Single-Walled Boron Nitride Nanotubes Conveying Fluid in Thermal Environment Via Nonlocal Strain Gradient Shell Model

P. Roodgar Saffari [1], M. Fakhraie [1,*], M.A. Roudbari [2]

[1]*Department of Mechanical Engineering, Lahijan Branch, Islamic Azad University, Lahijan, Iran*
[2]*School of Engineering, RMIT University, PO Box 71, Bundoora, VIC, 3083, Australia*

Received 21 February 2021; accepted 11 April 2021

ABSTRACT

The free vibration behavior of two fluid-conveying vertically-aligned single-walled boron nitride nanotubes are studied in the present paper via the nonlocal strain gradient piezoelectric theory in conjunction with the first-order shear deformation shell assumption in thermal environments. It is supposed that the two adjacent boron nitride nanotubes are coupled with each other in the context of linear deformation by van der Waals interaction according to Lennard–Jones potential function. To achieve a more accurate modeling for low-scale structures, both hardening and softening effects of materials are considered in the nonlocal strain gradient approach. The motion equations and associated boundary conditions are derived by means of Hamilton's variational principle, then solved utilizing differential quadrature method. Numerical studies are done to reveal the effect of different boundary conditions, size scale parameters, aspect ratio, inter-tube distance, and temperature change on the variations of dimensionless eigenfrequency and critical flow velocity.

© 2021 IAU, Arak Branch. All rights reserved.

Keywords: Nonlocal strain gradient; Fluid-conveying boron nitride nanotube; Free vibration; Piezoelectric cylindrical shell; Thermal environment.

1 INTRODUCTION

As a consequence of providing attractive mechanical, electrical and physical properties, nanotubes (NTs) have been utilized for various advanced applications in nanostructures [1]. Undoubtedly, one of the most notable carbon allotropes is carbon nanotube (CNT) including rolled-up single-walled carbon nanotubes (SWCNTs) or multi-walled carbon nanotubes (MWCNTs) [2, 3]. Boron nitride (BN) is a chemically resilient refractory mixture of boron and nitrogen atoms which has numerous outstanding characteristics including a high elastic modulus, and noteworthy efficiency in heat transfer fields [4, 5]. An advantages of boron nitride nanotubes (BNNTs) over CNT is

*Corresponding author. Tel.: +98 9111321248.
E-mail address: fakhraie@liau.ac.ir (M.Fakhraie)

© 2021 IAU, Arak Branch. All rights reserved.

that BNNTs exhibit strong piezoelectric properties which makes them an interesting choice in nano-electromechanical systems (NEMS) [6]. Some researchers have investigated the static and dynamic behavior of BNNTs. For example, based on the Donnell shell approach, Salehi-Khojin and Jalili [7] studied the buckling behavior of multi-walled BNNTs (MWBNNTs)-based composites corresponding to electro-thermo-mechanical loadings. By taking into account molecular mechanics simulations and continuum mechanics assumptions, Chowdhury et al. [8] carried out the transverse and radial breathing vibrations of armchair and zigzag BNNTs. The critical buckling loads of BNNTs for different diameters subjected to uniaxial compression loading were obtained via the molecular dynamic (MD) by Ebrahimi-Nejad et al. [9]. Yang et al. [10] analyzed the influence of geometrically nonlinear deformation on the nonlinear dynamic response of piezoelectric cylindrical shells reinforced using BNNTs via the finite difference technique. A three dimensional finite element method was applied by Ansari et al. [11] to investigate the stability properties of single-walled BNNTs (SWBNNTs) and demonstrated that zigzag BNNTs offer more stability than armchair ones. Recently, Yan et al. [12] studied the influence of tube-shaped radius on the frequencies of both torsional and longitudinal free vibrations of BNNTs. Owing to the significance of low-size structures, numerous empirical tests and atomistic simulations [13, 14] have been performed to show the noteworthy impact of low-size materials on mechanical properties as the material size enters the nanoscale. Due to the existing issues such as great computational costs in utilizing controlled tests and MD modelling in nanostructures and the lack of an internal length scale factor in traditional continuum models, higher-order non-classical continuum approaches are required to perfectly predict the mechanical behavior of low-size structures [15–23]. Until now, several projects have utilized the described non-classical continuum models to consider the impacts of low scale on the free/forced vibration, and the static/dynamic instability problem of different CNTs and BNNTs [24–43]. For example, by taking into account the nonlocal elasticity theory of Eringen [21] in the framework of Euler–Bernoulli beam assumption, Ghorbanpour Arani and Roudbari [44] proposed a non-classical model to study the impacts of surface stress and small scale on the nonlocal frequencies of zigzag coupled SWBNNT via viscoelastic medium. Regarding the concept of nonlocal elasticity theory, the stress state at every point of the area of nanostructures is supposed to be a function of strain states at all other points of the nanostructure. Mercan and Civalek [45] obtained the buckling load of BNNTs on elastic substrate aided by the nonlocal elasticity theory with discrete singular convolution (DSC). Akgöz and Civalek [46] applied the modified strain gradient theory introduced by Lam et al. [22] to investigate the bending of SWCNTs based on a higher-order beam model. According to the modified strain gradient theory, to exactly capture the effect of low scale, three independent higher-order length scale parameters should be considered. To consider both hardening and softening effects in a single theory, Lim et al. [47] combined the nonlocal elasticity and strain gradient approaches and demonstrated that to achieve a correct modeling of the size-dependent structures, it is essential to employ both hardening and softening effects of materials. The proposed non-classical assumption is the so-called nonlocal strain gradient theory (NSGT). When using NSGT, rhe focus is on correctly considering the influence of two length scale terms on the physical and mechanical behaviors of size-dependent structures. Li et al. [48] applied NSGT in the framework of Euler–Bernoulli beam theory to analyze the flexural wave propagation phenomenon through functionally graded nanobeams. The authors indicated that the acoustical and optical phase velocities normally increase with decreasing nonlocal factor or increasing material length scale term. In another study by Li et al. [49], wave propagation problem in size-dependent SWCNT in view of surface effect and magnetic field was carried out via NSGT. Malikan et al. [50] showed how the thermal environment affects the forced vibration of SWCNTs resting on viscoelastic foundation using NSGT. Dehghan et al. [51] studied the small size effect on the wave propagation problem of fluid-conveying magneto-electro-elastic nanotube via NSGT. Recently, Mohammadian et al. [52] used NSGT in the framework of Euler-Bernoulli beam model to investigate the natural frequencies of hetero-junction CNTs. Thanks to impeccable hollow cylindrical geometry in CNTs and BNNTs along with amazing chemical, mechanical and physical characteristics, they are anticipated to be utilized as nanofluidic, gas storage, and drug delivery systems [53–59]. Ghorbanpour-Arani et al. [60] reported size-dependent wave propagation in double-walled BNNTs conveying nanoflow based on nonlocal Timoshenko beam theory. NSGT in conjunction with the shear deformable shell theory was used by Zeighampour et al. [61] to investigate wave propagation in fluid-conveying double walled CNTs considering Van Der Waals (VDW) force between the two intended walls. Mohammadi et al. [62] applied NSGT in conjunction with cylindrical shell model to study the free vibration of an SWCNT conveying viscous fluid. The free vibration and instability behavior of SWCNT conveying viscous fluid flow were investigated by Mahinzare et al. [63] via NSGT and firs-order shear deformation theory.

The above literature review evidently shows that no analytical or numerical study on the application of NSGT in conjunction with first-order shear deformation shell model has been carried out to examine the vibration behavior of two vertically-aligned SWBNNTs conveying fluid in thermal environment. Therefore, the major purpose of current paper is to fill this important gap in the literature. Indeed, investigations demonstrated that drugs could bind to the

© 2021 IAU, Arak Branch

BNNTs surface in a stable manner with non-covalent interactions. Also, BNNTs are biocompatible and non-toxic, and have the potential to act as competent drug delivery vehicles. Therefore, one of the main innovations of the present work is to consider the effect of VDW interaction between two SWBNNTs conveying nanofluid with respect to the variations of temperature and external voltage. On the other hand, the effect of size-dependency on the dynamic behavior of BNNTs is presented by implementing both hardening and softening effects in the framework of NSGT. The first-order shear deformation shell model which include the effects of transverse shear deformation and rotary inertia is considered for obtaining the governing equations of motion. The two vertically-aligned SWBNNTs are coupled through VDW interaction. The motion equations and associated boundary conditions are derived by means of Hamilton's variational principle, and then solved utilizing differential quadrature method (DQM). As mode shapes are very important in the design of the smart nanostructures. Thus, the effect of small scale parameters on the mode shapes of various boundary conditions are investigated. Furthermore, it is denoted that VDW force is a substantial parameter and cannot be neglected in the analysis.

2 PRELIMINARY FORMULATION

As schematically demonstrated in Fig. 1, two vertically-aligned SWBNNTs (simulated as cylindrical shell) of the ensemble network conveying fluid and of the same length L, same radius R, same mean radius r_m, inter-tube distance l_m, and same uniform thickness h are subjected to the thermal environment of ΔT .

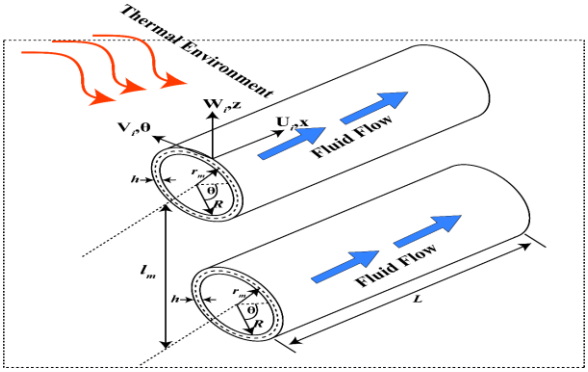

Fig.1
Two vertically-aligned SWBNNTs conveying fluid subjected to temperature change.

Based on the first-order shear deformable shell approach, the deflection field (*U, V, W*) for the cylindrical shell can be expressed as [64-66]:

$$\begin{aligned} U_i(x,\theta,z,t) &= u_i(x,\theta,t) + z\,\psi_{xi}(x,\theta,t), \\ V_i(x,\theta,z,t) &= v_i(x,\theta,t) + z\,\psi_{\theta i}(x,\theta,t), \\ W_i(x,\theta,z,t) &= w_i(x,\theta,t), \quad i = 1,2. \end{aligned} \tag{1}$$

In which *u, v* and *w* refer to the displacements along the curvilinear coordinates x, θ and z, respectively. Furthermore, ψ_x and ψ_θ indicate the rotations of each BNNT cross-section about $x-$ and $\theta-$ axis. Based on the displacement field stated in Eq. (1) and implemented linear strain-displacement relations, the nonzero strains can be presented as:

$$\begin{aligned} \varepsilon_{xxi} &= \frac{\partial u_i}{\partial x} + z\,\frac{\partial \psi_{xi}}{\partial x}, \\ \varepsilon_{\theta\theta i} &= \frac{1}{R}\frac{\partial v_i}{\partial \theta} + \frac{z}{R}\frac{\partial \psi_{\theta i}}{\partial \theta} + \frac{w_i}{R}, \\ \gamma_{x\theta i} &= \frac{\partial v_i}{\partial \theta} + \frac{1}{R}\frac{\partial u_i}{\partial \theta} + z\left(\frac{1}{R}\frac{\partial \psi_{xi}}{\partial \theta} + \frac{\partial \psi_{\theta i}}{\partial x}\right), \end{aligned} \tag{2}$$

© 2021 IAU, Arak Branch

$$\begin{aligned}\gamma_{\theta zi} &= \psi_{\theta i} + \frac{1}{R}\frac{\partial w_i}{\partial \theta} - \frac{v_i}{R},\\ \gamma_{xzi} &= \frac{\partial w_i}{\partial x} + \psi_{xi}.\end{aligned} \tag{2}$$

The non-classical differential constitutive equation based on the assumption of Lim et al. [47] in the framework of piezoelectricity theory can be expressed as:

$$\begin{aligned}&\left[1-(e_0\alpha)^2\left(\frac{\partial^2}{\partial x^2}+\frac{1}{R^2}\frac{\partial^2}{\partial\theta^2}\right)\right]\begin{bmatrix}\sigma_{xxi}\\ \sigma_{\theta\theta i}\\ \sigma_{x\theta i}\\ \sigma_{\theta zi}\\ \sigma_{xzi}\end{bmatrix} =\\ &\left[1-l^2\left(\frac{\partial^2}{\partial x^2}+\frac{1}{R^2}\frac{\partial^2}{\partial\theta^2}\right)\right]\left\{\begin{bmatrix}\frac{E}{1-\vartheta^2} & \frac{\vartheta E}{1-\vartheta^2} & 0 & 0 & 0\\ \frac{\vartheta E}{1-\vartheta^2} & \frac{E}{1-\vartheta^2} & 0 & 0 & 0\\ 0 & 0 & \frac{E}{2(1+\vartheta)} & 0 & 0\\ 0 & 0 & 0 & \frac{E}{2(1+\vartheta)} & 0\\ 0 & 0 & 0 & 0 & \frac{E}{2(1+\vartheta)}\end{bmatrix}\begin{bmatrix}\varepsilon_{xxi}\\ \varepsilon_{\theta\theta i}\\ \gamma_{x\theta i}\\ \gamma_{\theta zi}\\ \gamma_{xzi}\end{bmatrix}-\right.\\ &\left.\begin{bmatrix}0 & 0 & e_{31}\\ 0 & 0 & e_{31}\\ 0 & 0 & 0\\ 0 & e_{24} & 0\\ e_{24} & 0 & 0\end{bmatrix}\begin{bmatrix}E_{xi}\\ E_{\theta i}\\ E_{zi}\end{bmatrix}-\begin{bmatrix}\alpha\\ \alpha\\ 0\\ 0\\ 0\end{bmatrix}\Delta T\right\},\\ &\left[1-(e_0\alpha)^2\left(\frac{\partial^2}{\partial x^2}+\frac{1}{R^2}\frac{\partial^2}{\partial\theta^2}\right)\right]\begin{bmatrix}D_{xi}\\ D_{\theta i}\\ D_{zi}\end{bmatrix} =\\ &\left[1-l^2\left(\frac{\partial^2}{\partial x^2}+\frac{1}{R^2}\frac{\partial^2}{\partial\theta^2}\right)\right]\left[\begin{bmatrix}0 & 0 & 0 & 0 & e24\\ 0 & 0 & 0 & e_{24} & 0\\ e_{31} & e_{31} & 0 & 0 & 0\end{bmatrix}\begin{bmatrix}\varepsilon_{xxi}\\ \varepsilon_{\theta\theta i}\\ \gamma_{x\theta i}\\ \gamma_{\theta zi}\\ \gamma_{xzi}\end{bmatrix}-\right.\\ &\left.\begin{bmatrix}S_{11} & 0 & 0\\ 0 & S_{22} & 0\\ 0 & 0 & S_{33}\end{bmatrix}\begin{bmatrix}E_{xi}\\ E_{\theta i}\\ E_{zi}\end{bmatrix}+\begin{bmatrix}p_1\\ p_2\\ p_3\end{bmatrix}\Delta T\right].\end{aligned} \tag{3}$$

where $\begin{bmatrix}\sigma_{xx} & \sigma_{\theta\theta} & \sigma_{x\theta} & \sigma_{\theta z} & \sigma_{xz}\end{bmatrix}^T$ denotes the stress tensor, $\begin{bmatrix}D_x & D_\theta & D_z\end{bmatrix}^T$ is the electric displacement, and $\begin{bmatrix}E_x & E_\theta & E_z\end{bmatrix}^T$ represents the electric field vector. The symbol E refers to the Young's

© 2021 IAU, Arak Branch

modulus of BNNT. Furthermore, the parameters $e_0 a$ and l denote, respectively, the nonlocal term and the strain gradient term. Moreover, e_0 and a represent, respectively, the calibration constant and the internal characteristic length. Also, α is the thermal expansion coefficient, and the thermal changes of the environment is demonstrated by ΔT . Moreover, ϑ is Poisson's ratio and e_{ij} ,s_{ij} and p_i are, respectively, reduced piezoelectric constants, dielectric constants and pyroelectric constants.

Based on the piezoelectricity theory [67], the electric potential for each SWBNNT can be defined as:

$$\phi(x,\theta,z,t) = -\cos\left(\frac{\pi z}{h}\right)\varphi_i(x,\theta,t) + \frac{2zV_0}{h},\ i = 1,2. \tag{4}$$

In which φ_i denotes the variation of electric potential for each SWBNNT and V_0 expresses the external electric voltage. However, to satisfy Maxwell relations, the electric field must be considered as:

$$\begin{aligned} E_x &= -\frac{\partial\phi}{\partial x} = \cos\left(\frac{\pi z}{h}\right)\frac{\partial\varphi}{\partial x}, \\ E_\theta &= -\frac{1}{R+z}\frac{\partial\phi}{\partial y} = \frac{1}{R+z}\cos\left(\frac{\pi z}{h}\right)\frac{\partial\varphi}{\partial x}, \\ E_z &= -\frac{\partial\phi}{\partial z} = -\frac{\pi}{h}\sin\left(\frac{\pi z}{h}\right)\varphi - 2\frac{V_0}{h}. \end{aligned} \tag{5}$$

Hamilton's principle is employed to derive the governing equations and boundary conditions according to [68]

$$\int_0^t \delta(\Pi_s + \Pi_f - \Pi_k)dt = 0 \tag{6}$$

where Π_s , Π_f and Π_k are the virtual strain energy term, the work done by external forces (the work exerted by fluid-SWBNNT interaction, external electric potential and temperature rise, and vdW forces) and the kinetic energy, respectively. The strain energy variation of the fluid-conveying SWBNNTs is written as:

$$\begin{aligned} \delta\Pi_S = &\int_0^{2\pi}\int_0^L \int_{-\frac{h}{2}}^{\frac{h}{2}} \left[\sigma_{xx1}\delta\varepsilon_{xx1} + \sigma_{\theta\theta1}\delta\varepsilon_{\theta\theta1} + \sigma_{x\theta1}\delta\gamma_{x\theta1} + \sigma_{\theta z1}\delta\gamma_{\theta z1} + \sigma_{xz1}\delta\gamma_{xz1} - \right. \\ &\left. D_{x1}\delta E_{x1} - D_{\theta1}\delta E_{\theta1} - D_{z1}\delta E_{z1}\right] R\,dx\,d\theta\,dz + \\ &\int_0^{2\pi}\int_0^L \int_{-\frac{h}{2}}^{\frac{h}{2}} \left[\sigma_{xx2}\delta\varepsilon_{xx2} + \sigma_{\theta\theta2}\delta\varepsilon_{\theta\theta2} + \sigma_{x\theta2}\delta\gamma_{x\theta2} + \sigma_{\theta z2}\delta\gamma_{\theta z2} + \sigma_{xz2}\delta\gamma_{xz2} - \right. \\ &\left. D_{x2}\delta E_{x2} - D_{\theta2}\delta E_{\theta2} - D_{z2}\delta E_{z2}\right] R\,dx\,d\theta\,dz \end{aligned} \tag{7}$$

Substituting Eq. (2) into Eq. (7) results in the following set of equations:

$$\begin{aligned} &\int_0^{2\pi}\int_0^L \left[N_{xx1}\delta\frac{\partial u_1}{\partial x} + M_{xx1}\delta\frac{\partial\psi_{x1}}{\partial x} + N_{\theta\theta1}\delta\left(\frac{1}{R}\frac{\partial v_1}{\partial\theta} + \frac{1}{R}W_1\right) + \frac{1}{R}M_{\theta\theta1}\delta\frac{\partial\psi_{\theta1}}{\partial\theta} + \right. \\ &N_{x\theta1}\delta\left(\frac{\partial v_1}{\partial x} + \frac{1}{R}\frac{\partial u_1}{\partial\theta}\right) + M_{x\theta1}\delta\left(\frac{1}{R}\frac{\partial\psi_{x1}}{\partial\theta} + \frac{\partial\psi_{\theta1}}{\partial x}\right) + Q_{\theta z1}\delta\left(\psi_{\theta1} - \frac{1}{R}\frac{\partial w_1}{\partial\theta} - \frac{v_1}{R}\right) + \\ &\left. Q_{xz1}\delta\left(\psi_{x1} + \frac{\partial w_1}{\partial\theta}\right)\right] R\,dx\,d\theta - \end{aligned} \tag{8}$$

© 2021 IAU, Arak Branch

$$\int_0^{2\pi}\int_0^L\int_{-\frac{h}{2}}^{\frac{h}{2}}\left[D_{x1}\delta E_{x1}+D_{\theta 1}\delta E_{\theta 1}+D_{z1}\delta E_{z1}\right]Rdxd\theta dz+\int_0^{2\pi}\int_0^L\left[N_{xx2}\delta\frac{\partial u_2}{\partial x}+\right.$$
$$M_{xx1}\delta\frac{\partial\psi_{x2}}{\partial x}+N_{\theta\theta 2}\delta\left(\frac{1}{R}\frac{\partial v_2}{\partial\theta}+\frac{1}{R}W_2\right)+\frac{1}{R}M_{\theta\theta 2}\delta\frac{\partial\psi_{\theta 2}}{\partial\theta}+N_{x\theta 2}\delta\left(\frac{\partial v_2}{\partial x}+\frac{1}{R}\frac{\partial u_2}{\partial\theta}\right)+$$
$$M_{x\theta 2}\delta\left(\frac{1}{R}\frac{\partial\psi_{x2}}{\partial\theta}+\frac{\partial\psi_{\theta 2}}{\partial x}\right)+Q_{\theta z2}\delta\left(\psi_{\theta 2}+\frac{1}{R}\frac{\partial w_2}{\partial\theta}-\frac{v_2}{R}\right)+Q_{xz2}\delta\left(\psi_{x2}+\right. \tag{8}$$
$$\left.\left.\frac{\partial w_2}{\partial x}\right)\right]Rdxd\theta-\int_0^{2\pi}\int_0^L\int_{-\frac{h}{2}}^{\frac{h}{2}}\left[D_{x2}\delta E_{x2}+D_{\theta 2}\delta E_{\theta 2}+D_{z2}\delta E_{z2}\right]Rdxd\theta dz$$

where $N_{xxi}, M_{xxi}, N_{\theta\theta i}, M_{\theta\theta i}, N_{x\theta i}, M_{x\theta i}, Q_{\theta zi}, Q_{xzi}$ denote the bending moments and shear forces, defined as:

$$\left\langle N_{xxi}, N_{\theta\theta i}, N_{x\theta i}\right\rangle=\int_{-\frac{h}{2}}^{\frac{h}{2}}\left\langle Q_{xxi}, Q_{\theta\theta i}, Q_{x\theta i}\right\rangle dz,$$
$$\left\langle M_{xxi}, M_{\theta\theta i}, M_{x\theta i}\right\rangle=\int_{-\frac{h}{2}}^{\frac{h}{2}}\left\langle Q_{xxi}, Q_{\theta\theta i}, Q_{x\theta i}\right\rangle z\,dz, \tag{9}$$
$$\left\langle Q_{\theta zi}, Q_{xzi}\right\rangle=\int_{-\frac{h}{2}}^{\frac{h}{2}}k_s\left\langle\sigma_{\theta zi}, \sigma_{xzi}\right\rangle dz,$$

where k_s refers to the shear correction term.

The variation of kinetic energy using Eq. (1) can be presented as:

$$\delta\Pi_k=\int_0^{2\pi}\int_0^L\int_{-\frac{h}{2}}^{\frac{h}{2}}\rho\left[\frac{\partial u_1}{\partial t}\delta\frac{\partial u_1}{\partial t}+z\frac{\partial\psi_{x1}}{\partial t}\delta\frac{\partial u_1}{\partial t}+z\frac{\partial u_1}{\partial t}\delta\frac{\partial\psi_{x1}}{\partial t}+z^2\frac{\partial\psi_{x1}}{\partial t}\delta\frac{\partial\psi_{x1}}{\partial t}+\right.$$
$$\frac{\partial v_1}{\partial t}\delta\frac{\partial v_1}{\partial t}+z\frac{\partial\psi_{\theta 1}}{\partial t}\delta\frac{\partial v_1}{\partial t}+z\frac{\partial v_1}{\partial t}\delta\frac{\partial\psi_{\theta 1}}{\partial t}+z^2\frac{\partial\psi_{\theta 1}}{\partial t}\delta\frac{\partial\psi_{\theta 1}}{\partial t}+\frac{\partial w_1}{\partial t}\delta\frac{\partial w_1}{\partial t}\left.\right]Rdxd\theta dz+$$
$$\int_0^{2\pi}\int_0^L\int_{-\frac{h}{2}}^{\frac{h}{2}}\rho\left[\frac{\partial u_2}{\partial t}\delta\frac{\partial u_2}{\partial t}+z\frac{\partial\psi_{x2}}{\partial t}\delta\frac{\partial u_2}{\partial t}+z\frac{\partial u_2}{\partial t}\delta\frac{\partial\psi_{x2}}{\partial t}+z^2\frac{\partial\psi_{x2}}{\partial t}\delta\frac{\partial\psi_{x2}}{\partial t}+\frac{\partial v_2}{\partial t}\delta\frac{\partial v_2}{\partial t}+\right. \tag{10}$$
$$\left.z\frac{\partial\psi_{\theta 2}}{\partial t}\delta\frac{\partial v_2}{\partial t}+z\frac{\partial v_2}{\partial t}\delta\frac{\partial\psi_{\theta 2}}{\partial t}+z^2\frac{\partial\psi_{\theta 2}}{\partial t}\delta\frac{\partial\psi_{\theta 2}}{\partial t}+\frac{\partial w_2}{\partial t}\delta\frac{\partial w_2}{\partial t}\right]Rdxd\theta dz$$

where ρ stands for the density of each mass of SWBNNT. It should be noted that the fluid inside the every SWBNNT is taken as incompressible, inviscid, isentropic and irrotational. However, the external work variation exerted by fluid can be presented as:

$$\delta\Pi_{f,fluid}=\int_0^{2\pi}\int_0^L\rho_f\left[\left(\frac{\partial}{\partial t}+U\frac{\partial}{\partial x}\right)^2\right]w_1\delta w_1Rdxd\theta+\int_0^{2\pi}\int_0^L\rho_f\left[\left(\frac{\partial}{\partial t}+U\frac{\partial}{\partial x}\right)^2\right]w_2\delta w_2Rdxd\theta \tag{11}$$

In which ρ_f indicates the mass density of applied fluid. Furthermore, U represents the fluid velocity.

© 2021 IAU, Arak Branch

Also, according to Lennard–Jones potential function, the external work variation exerted by vdW forces on a SWBNNT, owing to its relative lateral motion with respect to its neighboring BNNT, can be defined as: [69, 70]

$$\delta\Pi_{f,vdw} = \int_0^{2\pi}\int_0^L C_z\left(w_1 - w_2\right)\delta w_1 R dx d\theta + \int_0^{2\pi}\int_0^L C_y\left(v_1 - v_2\right)\delta v_1 R dx d\theta - \int_0^{2\pi}\int_0^L C_z\left(w_1 - w_2\right)\delta w_2 R dx d\theta - \int_0^{2\pi}\int_0^L C_y\left(v_1 - v_2\right)\delta v_2 R dx d\theta \tag{12}$$

where C_y and C_z express the VDW interaction factor, which are defined as: [69]

$$C_y = -\frac{256\in {r_m}^2}{9a^4 L}\int_0^L\int_0^L\int_0^{2\pi}\int_0^{2\pi}\left\langle \sigma^{12}\left[X^{-7} - 14X^{-8}\left\{r_m\left(\cos\Phi_2 - \cos\Phi_1\right)\right\}^2\right] - \frac{\sigma^6}{2}\left[X^{-4} - 8X^{-5}\left\{r_m\left(\cos\Phi_2 - \cos\Phi_1\right)\right\}^2\right]\right\rangle d\Phi_1 d\Phi_1 dx_1 dx_2,$$

$$C_z = -\frac{256\in {r_m}^2}{9a^4 L}\int_0^L\int_0^L\int_0^{2\pi}\int_0^{2\pi}\left\langle \sigma^{12}\left[X^{-7} - 14X^{-8}\left\{r_m\left(\sin\Phi_2 - \sin\Phi_1\right)\right\}^2\right] - \frac{\sigma^6}{2}\left[X^{-4} - 8X^{-5}\left\{d + r_m\left(\sin\Phi_2 - \sin\Phi_1\right)\right\}^2\right]\right\rangle d\Phi_1 d\Phi_1 dx_1 dx_2, \tag{13}$$

$$X = \left(x_2 - x_1\right)^2 + 2{r_m}^2\left\{1 - \cos\left(\Phi_2 - \Phi_1\right)\right\} + {l_m}^2 + 2r_m l_m\left(\sin\Phi_2 - \sin\Phi_1\right)$$

where $\in$ refers to the well depth, a is length of the BN bound, and σ denotes the equilibrium distance. Finally, the external work variation exerted by the electric potential and temperature rise for each SWBNNT can be written as:

$$\delta\Pi_{f,elec} = \int_0^{2\pi}\int_0^L\left[\left(N_x^T + N_E\right)\frac{\partial w_1}{\partial x}\delta\frac{\partial w_1}{\partial x}\right]R\,dx d\theta + \int_0^{2\pi}\int_0^L\left[\left(N_x^T + N_E\right)\frac{\partial v_1}{\partial x}\delta\frac{\partial v_1}{\partial x}\right]R\,dx d\theta + \int_0^{2\pi}\int_0^L\left[\left(N_x^T + N_E\right)\frac{\partial w_2}{\partial x}\delta\frac{\partial w_2}{\partial x}\right]R\,dx d\theta + \int_0^{2\pi}\int_0^L\left[\left(N_x^T + N_E\right)\frac{\partial v_2}{\partial x}\delta\frac{\partial v_2}{\partial x}\right]R\,dx d\theta \tag{14}$$

where

$$N_x^T = \int_{-\frac{h_1}{2}}^{\frac{h_1}{2}} E\,\alpha\Delta T dz,\quad N_E = -\int_{-\frac{h_1}{2}}^{\frac{h_1}{2}}\frac{2e_{31}V_0}{h_1}dz. \tag{15}$$

Finally, substituting $\delta\Pi_s, \delta\Pi_f = \delta\Pi_{f,fluid} + \delta\Pi_{f,vdW} + \delta\Pi_{f,elec}$ and $\delta\Pi_k$ in the Hamilton's principle, the general system of higher-order equations of motion can be obtained as:

$$\delta u_i : \frac{\partial N_{xxi}}{\partial x} + \frac{1}{R}\frac{\partial N_{x\theta i}}{\partial\theta} = I_0\frac{\partial^2 u_i}{\partial t^2} + I_1\frac{\partial^2\psi_{xi}}{\partial t^2}, \tag{16}$$

$$\delta v_1 : \frac{\partial N_{x\theta i}}{\partial x} + \frac{1}{R}\frac{\partial N_{\theta\theta i}}{\partial\theta} + \frac{Q_{\theta zi}}{R} - \left(N_x^T + N_E\right)\frac{\partial^2 v_i}{\partial x^2} + C_y\left(v_i - v_j\right) = I_0\frac{\partial^2 v_i}{\partial t^2} + I_1\frac{\partial^2\psi_{\delta\theta i}}{\partial t^2}, \tag{17}$$

© 2021 IAU, Arak Branch

$$\delta w_i : \frac{\partial Q_{xzi}}{\partial x} + \frac{1}{R}\frac{\partial Q_{\theta zi}}{\partial \theta} - \frac{N_{\theta\theta zi}}{R} - \rho_f \left(\frac{\partial^2 w_i}{\partial t^2} + 2U \frac{\partial^2 w_i}{\partial x\, \partial t} + U^2 \frac{\partial^2 w_i}{\partial x^2} \right) + C_z \left(w_i - w_j \right) - \left(N_x^T + N_E \right) \frac{\partial^2 w_i}{\partial x^2} = I_0 \frac{\partial^2 w_i}{\partial t^2}, \tag{18}$$

$$\delta \psi_{xi} : \frac{\partial M_{xxi}}{\partial x} + \frac{1}{R}\frac{\partial M_{x\theta i}}{\partial \theta} - Q_{xzi} = I_1 \frac{\partial^2 u_i}{\partial t^2} + I_2 \frac{\partial^2 \psi_{xi}}{\partial t^2}, \tag{19}$$

$$\delta \psi_{\theta i} : \frac{1}{R}\frac{\partial M_{\theta\theta i}}{\partial \theta} + \frac{1}{R}\frac{\partial M_{x\theta i}}{\partial x} - Q_{\theta zi} = I_1 \frac{\partial^2 v_i}{\partial t^2} + I_2 \frac{\partial^2 \psi_{\theta i}}{\partial t^2}, \tag{20}$$

$$\delta \varphi_i : \int_{-\frac{h}{2}}^{\frac{h}{2}} \left[\frac{\partial D_{xi}}{\partial x} \cos\left(\frac{\pi z}{h} \right) + \frac{1}{R+z} \frac{\partial D_{\theta i}}{\partial \theta} \cos\left(\frac{\pi}{h} \right) + D_{zi} \left(\frac{\pi}{h} \right) \sin\left(\frac{\pi z}{h} \right) \right] dz, \; i = 1,2 \tag{21}$$

In which

$$\left\langle I_0, I_1, I_2 \right\rangle = \int_{-\frac{h_1}{2}}^{\frac{h_1}{2}} \rho \left\langle 1, z, z^2 \right\rangle dz, \tag{22}$$

Also, Hamilton's principle gives the corresponding boundary conditions at each SWBNNT ends $\left(x = 0, L \right)$ as:

$$\delta u_i : N_{xxi} - \frac{1}{R}\frac{\partial N_{x\theta i}}{\partial \theta} = 0, \tag{23}$$

$$\delta v_1 : N_{x\theta i} - \frac{1}{R}\frac{\partial N_{\theta\theta i}}{\partial \theta} - \frac{Q_{\theta zi}}{R} = 0, \tag{24}$$

$$\delta w_i : Q_{xzi} - \frac{1}{R}\frac{\partial Q_{\theta zi}}{\partial \theta} + \frac{N_{\theta\theta i}}{R} = 0, \tag{25}$$

$$\delta \psi_{xi} : M_{xxi} - \frac{1}{R}\frac{\partial M_{x\theta i}}{\partial \theta} + Q_{xzi} = 0, \tag{26}$$

$$\delta \psi_{\theta i} : \frac{1}{R}\frac{\partial M_{\theta\theta i}}{\partial \theta} - M_{x\theta i} + Q_{\theta zi} = 0, \tag{27}$$

$$\delta \varphi_i : \int_{-\frac{h}{2}}^{\frac{h}{2}} \left[D_{xi} \cos\left(\frac{\pi z}{h} \right) \right] dz = 0, \; i = 1,2 \tag{28}$$

Finally, substituting Eq. (3) (with respect to Eq. 9) into Eqs. (16)–(21), the non-classical equilibrium equations in terms of displacements are derived and provided in Appendix A.

© 2021 IAU, Arak Branch

3 SOLUTION OF EQUATIONS OF FLUID _ CONVEYING SWBNNTs

To solve the set of main equations, i.e. equations given in Appendix A, DQM is utilized to discretize the equilibrium equations and associated boundary conditions. According to this method, the partial derivative of a function at a given discrete point can be determined by a weighted linear combination of the function values at all grid points. However, the derivative of each optional function in an optional point can be rewritten at all intervals. Furthermore, based on Chebyshev points, the grid points are computed as: [71]

$$X_j = \frac{1}{2}\left(1-\cos\frac{(j-1)}{(N-1)}\pi\right),\ j=1,2,\ldots,N. \tag{29}$$

In which N depicts the entire number of grid points. Additionally, the pth-order differential operator is indicated as a finite series in the form

$$\frac{\partial^p\{u_i,v_i,w_i,\psi_{xi},\psi_{\theta i}\}}{\partial X^k} = \sum_{j=1}^{N} C_{kj}^{(p)}\{\bar{u}_i,\bar{v}_i,\bar{w}_i,\bar{\psi}_{xi},\bar{\psi}_{\theta i}\}. \tag{30}$$

where $C_{kj}^{(p)}$ denotes the weighting factors for the pth-order derivative. In addition, the considered boundary conditions can be presented as:

$$u_i = v_i = w_i = \psi_{xi} = \psi_{\theta i} = \varphi_i = 0, \qquad x = 0, L \tag{31}$$

For a clamped-end (C) SWBNNT,

$$\begin{aligned} &v_i = w_i = \psi_{\theta i} = \varphi_i = 0, \qquad x = 0, L \\ &\left(1-l^2\frac{\partial^2}{\partial x^2}+\frac{l^2}{R^2}\frac{\partial^2}{\partial\theta^2}\right)\left(A_{11}\frac{\partial u_i}{\partial x}+B_{11}\frac{\partial\psi_{xi}}{\partial x}+A_{12}\left(\frac{\partial v_i}{R\partial\theta}+\frac{w_i}{R}\right)+B_{12}\frac{\partial\psi_{\theta i}}{R\partial\theta}\right)=0, \\ &\left(1-l^2\frac{\partial^2}{\partial x^2}+\frac{l^2}{R^2}\frac{\partial^2}{\partial\theta^2}\right)\left(\mathbf{B}_{11}\frac{\partial u_i}{\partial x}+D_{11}\frac{\partial\psi_{xi}}{\partial x}+B_{12}\left(\frac{\partial v_i}{R\partial\theta}+\frac{w_i}{R}\right)+D_{12}\frac{\partial\psi_{\theta i}}{R\partial\theta}\right)=0, \end{aligned} \tag{32}$$

For simply-supported-end (S) SWBNNT.

In order to investigate the free vibration of the two vertically-aligned SWBNNTs (simulated as cylindrical shell) of the ensemble network, the displacement field along the $\theta-$ direction can be stated as follows:

$$\begin{bmatrix} u_i(x,\theta,t) \\ v_i(x,\theta,t) \\ w_i(x,\theta,t) \\ \psi_{xi}(x,\theta,t) \\ \psi_{\theta i}(x,\theta,t) \\ \varphi_i(x,\theta,t) \end{bmatrix} = \sum_{n=1}^{\infty} e^{\omega t} \begin{bmatrix} \bar{u}_i(x)\cos(n\theta) \\ \bar{v}_i(x)\sin(n\theta) \\ \bar{w}_i(x)\cos(n\theta) \\ \bar{\psi}_{xi}(x)\cos(n\theta) \\ \bar{\psi}_{\theta i}(x)\sin(n\theta) \\ \bar{\varphi}_i(x)\cos(n\theta) \end{bmatrix} \tag{33}$$

where ω expresses the complex natural frequency. Firstly, substituting Eq. (33) into the governing equations (equations given in Appendix A) and related boundary conditions (Eqs. (31–32)), then employing DQM, the eigenvalue problem can be obtained as in the following matrix form

© 2021 IAU, Arak Branch

$$\left(M\,\omega^2+C\,\omega+K\right)d=0. \tag{34}$$

where ***M, C, K*** and ***d*** represent, respectively, the mass matrix, damping matrix, stiffness matrix, and modal vector. It must be noted that $Re(\omega)$ denotes the damping factor and $Im(\omega)$ expresses the natural frequency. Nevertheless, by attaining the non-trivial solution of relation (34), the complex natural eigenfrequency can be calculated.

4 RESULTS AND DISCUSSION

4.1 Convergence study

In this section, the convergence for performed calculations is systematically guaranteed in a simple trial and error fashion, i.e., by increasing the number of nodes distributed through the length of SWBNNTs, *N*, while seeking for stability in the predicted dimensionless complex natural frequencies with a predefined error bound $\left(\Delta\omega<10^{-7}\right)$. Therefore, the results stated in Table 1 indicate the convergence of the first two computed dimensionless natural frequencies $\left(\omega_{nom}=\omega R\sqrt{\frac{\rho}{E}}\right)$ for three various boundary conditions (i.e., CC, SC, and SS). As shown, at least 16 nodes (*N*=16) are required for the proper convergence of numerical solutions. Here, the length scale parameters are assumed to be zero. Also, the material and physical parameters of SWBNNTs used in this section and following ones (except for the section of verification of results) are in the form

$$\begin{aligned}
&E=18TPa,\ \rho=2300\frac{kg}{m^a},\ \vartheta=0.25,\ \rho_f=1000\frac{kg}{m^a},\ \alpha=1.6\times10^{-6},\\
&L=10R,\ R=12nm,\ h=0.05R,\ \in=4.20383,\ \sigma=0.34nm,\\
&a=0.145nm,\ \ rm=R+\frac{h}{2},\ lm=3nm,\ e_{31}=5.2,\ e_{24}=12.7,s_{11}=6.46\times10^{-9},\\
&s_{22}=6.46\times10^{-9},\ \ s_{33}=5.62\times10^{-9}.
\end{aligned} \tag{35}$$

Table 1
First two dimensionless natural frequencies with respect to the total number of nodes.

N	Mode	SS	CC
6	1	0.34246	0.95635
	2	0.79199	1.63742
8	1	0.35475	0.89507
	2	0.83139	1.43125
10	1	0.35856	0.88528
	2	0.83046	1.42668
12	1	0.35852	0.88520
	2	0.83042	1.42559
14	1	0.35851	0.88520
	2	0.83042	1.42559
16	1	0.35851	0.88520
	2	0.83042	1.42559

4.2 Comparison study

Before presenting the main results, the correctness and accuracy of the derived formulations must be established. To this end, by neglecting VDW force as well as fluid and thermal effect, the calculated values of the first natural frequencies of cylindrical piezoelectric shell for simply-supported boundary condition are reported in Table 2. Comparisons with numerical reports previously presented by Mehralian and Tadi Beni are also provided [72]. The

© 2021 IAU, Arak Branch

calculated frequency values demonstrate good agreement with the results presented in the mentioned study. Here, it is assumed that $L = R$, $\mu^2 = 3.3\,nm^2$ and $h = 0.05R$.

Table 2
Comparison study of the nondimensional natural frequencies (THz) of single cylindrical piezoelectric shell.

$l(nm)^2$	Present (DQM)	Ref. [72] (analytical)
0.1	0.3822	0.3813
0.3	0.5331	0.5323
0.5	0.6551	0.6542
0.7	0.7544	0.7536
0.9	0.8418	0.8409

4.3 Main results

Numerical studies are carried out in this section to properly understand the impact of several factors (i.e., size-dependent effects, inter-tube distance, aspect ratio, thermal environment) on the variations of the complex natural frequencies of the system.

In Fig. 2, the effect of the nonlocal term μ on the variations of the real and imaginary parts of eigenfrequency versus flow velocity for three various boundary conditions (i.e., SS, CC and CS) is displayed. Here, the strain gradient parameter and thermal factor are assumed to be zero, $L = 10R$, $V_0 = 0$ and $h = 0.05R$. The key observations are summarized as follows. As expected, the natural frequency (imaginary part of complex eigenfrequency) is reduced with increasing flow velocity until it becomes zero and the first mode of divergence instability occurs. One should note that the flow velocity related to the zero values of the imaginary part of frequency is named the critical velocity. It is also found that with increasing nonlocal factor, the natural frequency and critical flow velocity decrease for all boundary conditions. This is attributed to the fact that the interaction force between SWBNNT atoms decreases and brings about a softer system. On the other hand, the real part of complex eigenfrequency initially remains zero, meaning that in this period, the fluid flow in system does not experience any damping and the system is stable.

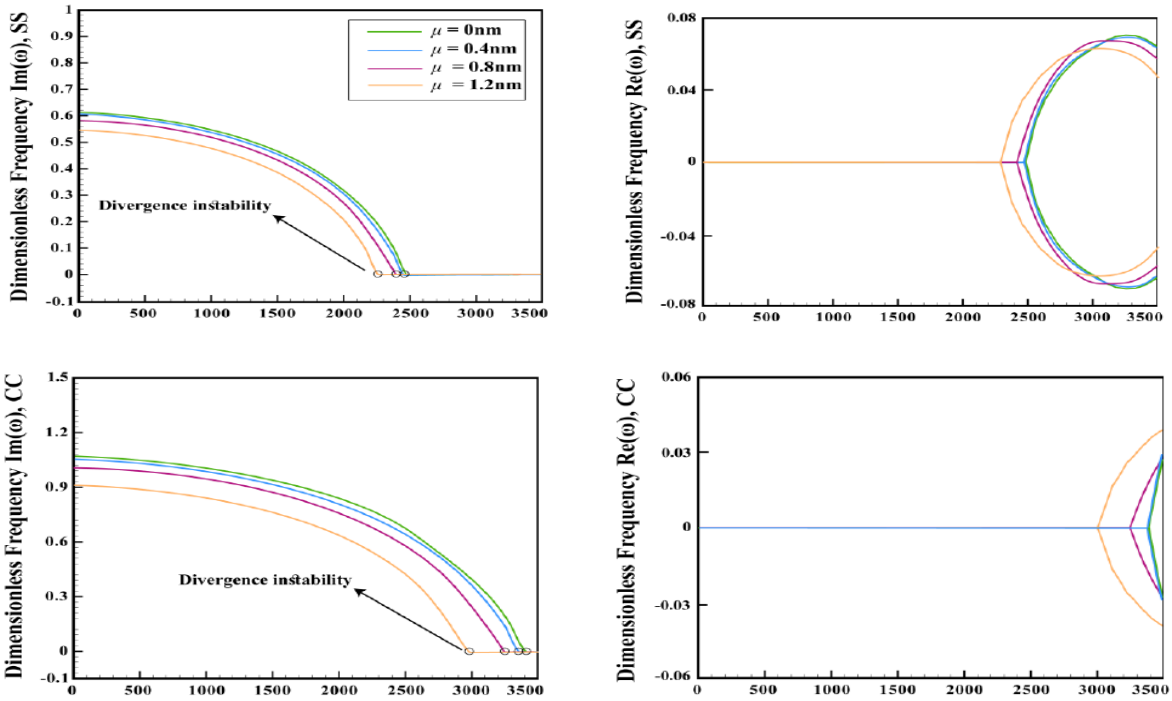

© 2021 IAU, Arak Branch

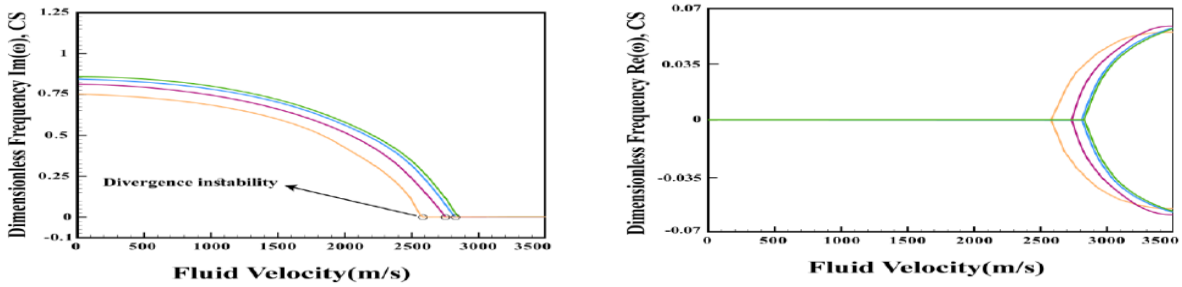

Fig.2
Effect of nonlocal term on the variations of the complex natural frequency versus flow velocity for different boundary conditions.

Fig. 3 shows the effect of strain gradient parameter on the variations of the imaginary and real parts of complex eigenfrequency with respect to different flow velocity values for different boundary conditions. Here, the nonlocal parameter and thermal factor are supposed to be zero, $L = 10R$, $V_0 = 0$ and $h = 0.05R$. The comments about divergence instability and critical flow velocity can readily be made similar to the mentioned remarks (i.e., as in Fig. 2). In particular, it is observed that as the strain gradient parameter increases, the natural frequency and critical flow velocity both increase since the interaction force between SWBNNT atoms increases and the structure becomes stiffer.

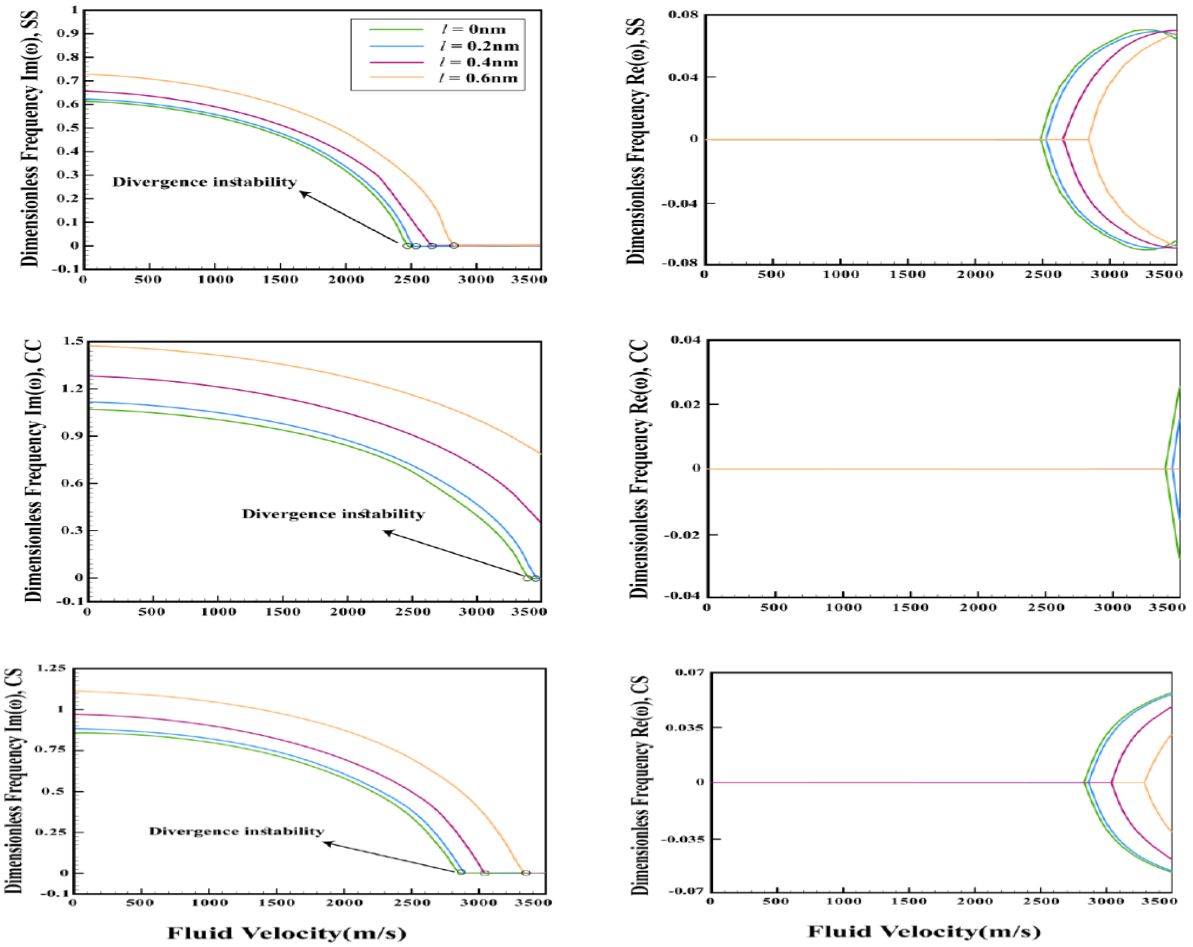

Fig.3
Effect of strain gradient parameter on the variations of the complex natural frequency versus flow velocity for different boundary conditions.

© 2021 IAU, Arak Branch

Fig. 4 demonstrates the effect of aspect ratio L/R on the variations of the imaginary part of dimensionless complex eigenfrequency against different flow velocity values for the first mode under various boundary conditions. Here, $\Delta T = 0$, $\mu = 0.4\,nm$, $l = 0.3\,nm$, and $V_0 = 0$. It is observed that with increasing aspect ratio, the natural frequency (imaginary part of complex eigenfrequency) and critical flow velocity are reduced. It is inferred that a system with a high aspect ratio is further likely to cause the divergence instability [73].

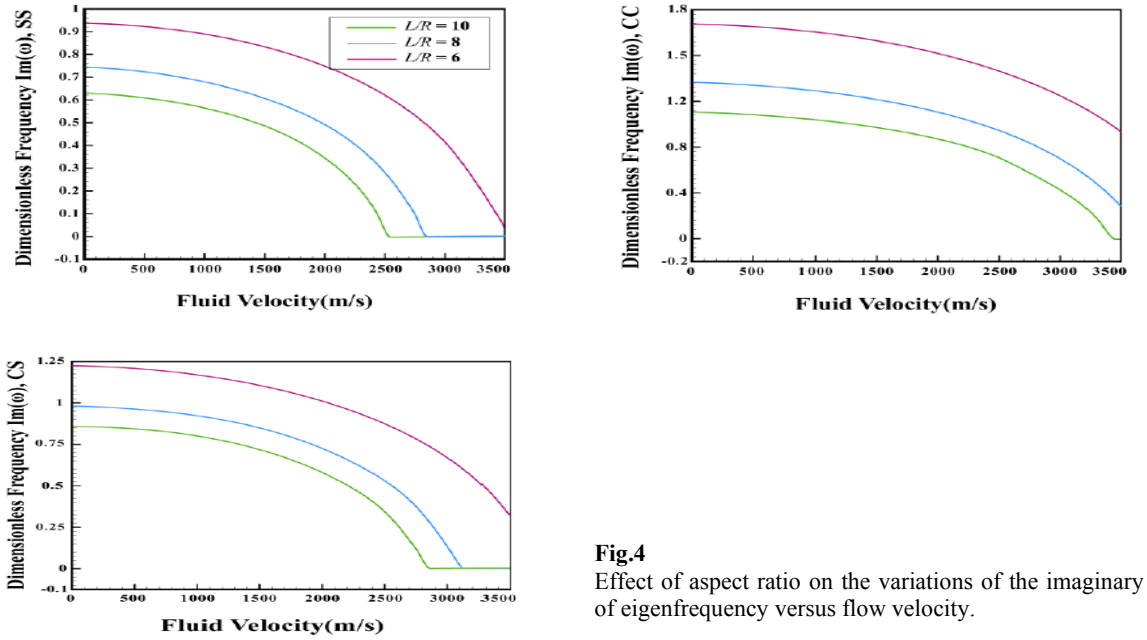

Fig.4
Effect of aspect ratio on the variations of the imaginary part of eigenfrequency versus flow velocity.

The effect of temperature on the imaginary part of the system eigenfrequency versus flow velocity for the first mode under various boundary conditions is displayed in Fig. 5. Here, $L/R = 10$, $\mu = 0.4\,nm$, $l = 0.3\,nm$ and $V_0 = 0$. The results indicate that an increase in temperature change leads to a higher natural frequency and critical flow velocity.

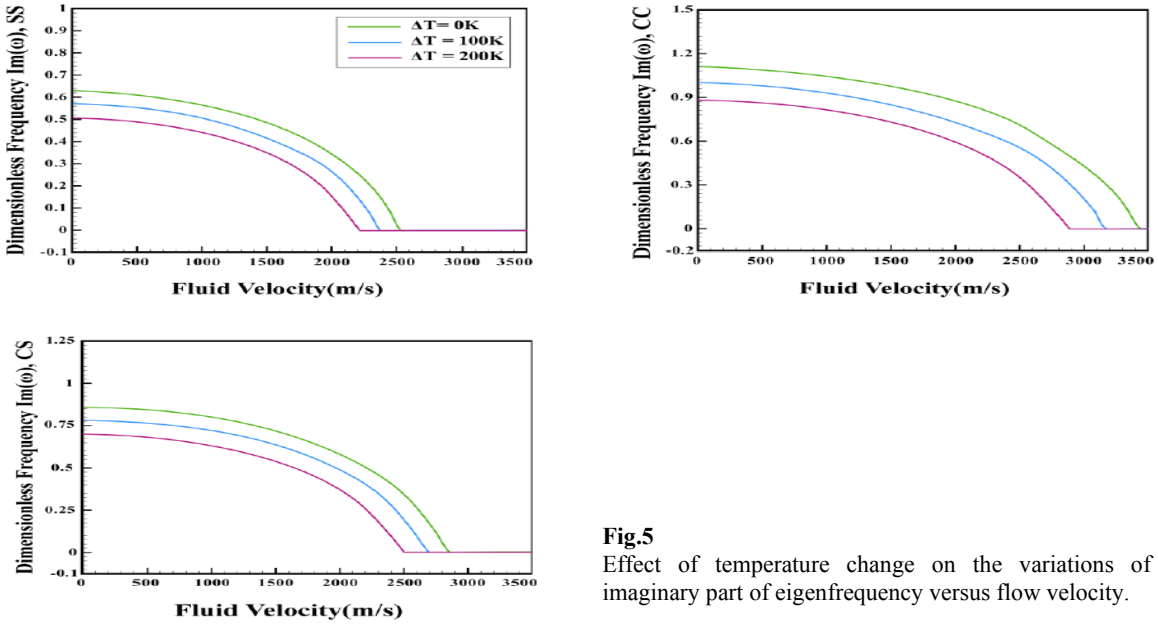

Fig.5
Effect of temperature change on the variations of the imaginary part of eigenfrequency versus flow velocity.

© 2021 IAU, Arak Branch

The influence of electric voltage on the imaginary part versus flow velocity for the first mode under various boundary conditions is depicted in Fig. 6. Here $L/R = 10,\ \Delta T = 0,\ \mu = 0.4\,nm$ and $l = 0.3\,nm$. It is shown that with increasing electric voltage, the natural frequency decreases.

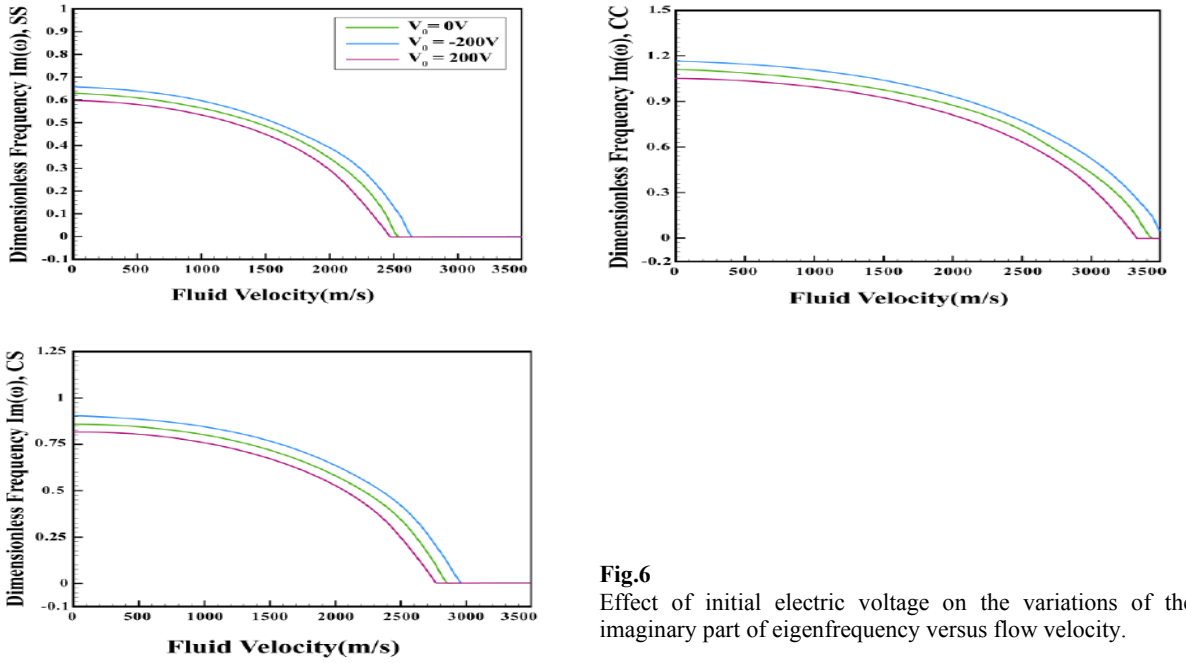

Fig.6
Effect of initial electric voltage on the variations of the imaginary part of eigenfrequency versus flow velocity.

The effect of inter-tube distance on the dimensionless frequency against flow velocity is presented in Fig. 7. Here, $L/R = 10,\ \Delta T = 0,\ \mu = 0.4\,nm,\ l = 0.3\,nm$ and $V_0 = 0$. As noted, the natural frequency decreases with increasing inter-tube distance of the two SWBNNTs. This result is in complete agreement with the findings of Ref. [66].

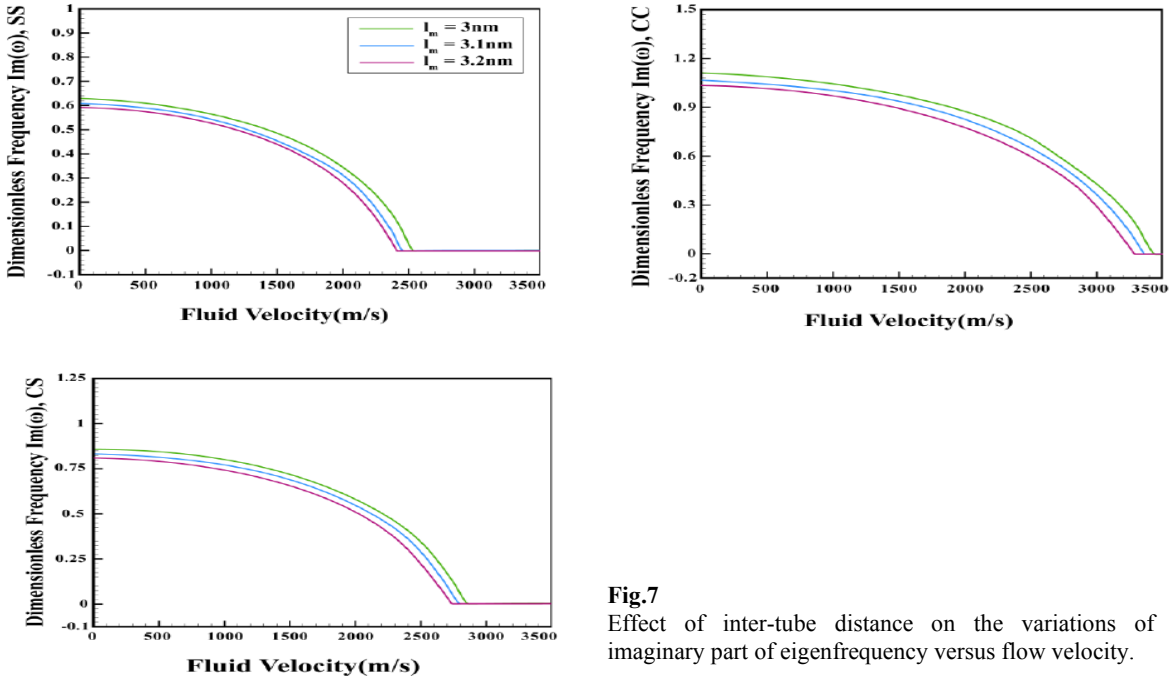

Fig.7
Effect of inter-tube distance on the variations of the imaginary part of eigenfrequency versus flow velocity.

© 2021 IAU, Arak Branch

Mode shapes are crucial in the design of smart nanostructures. Thus, the first three mode shapes of CC, SS, and CS boundary conditions are demonstrated in Fig. 8 for various values of the nonlocal and strain gradient parameters. In general, one concludes that the mode shapes of all boundary conditions are affected by small-scale terms.

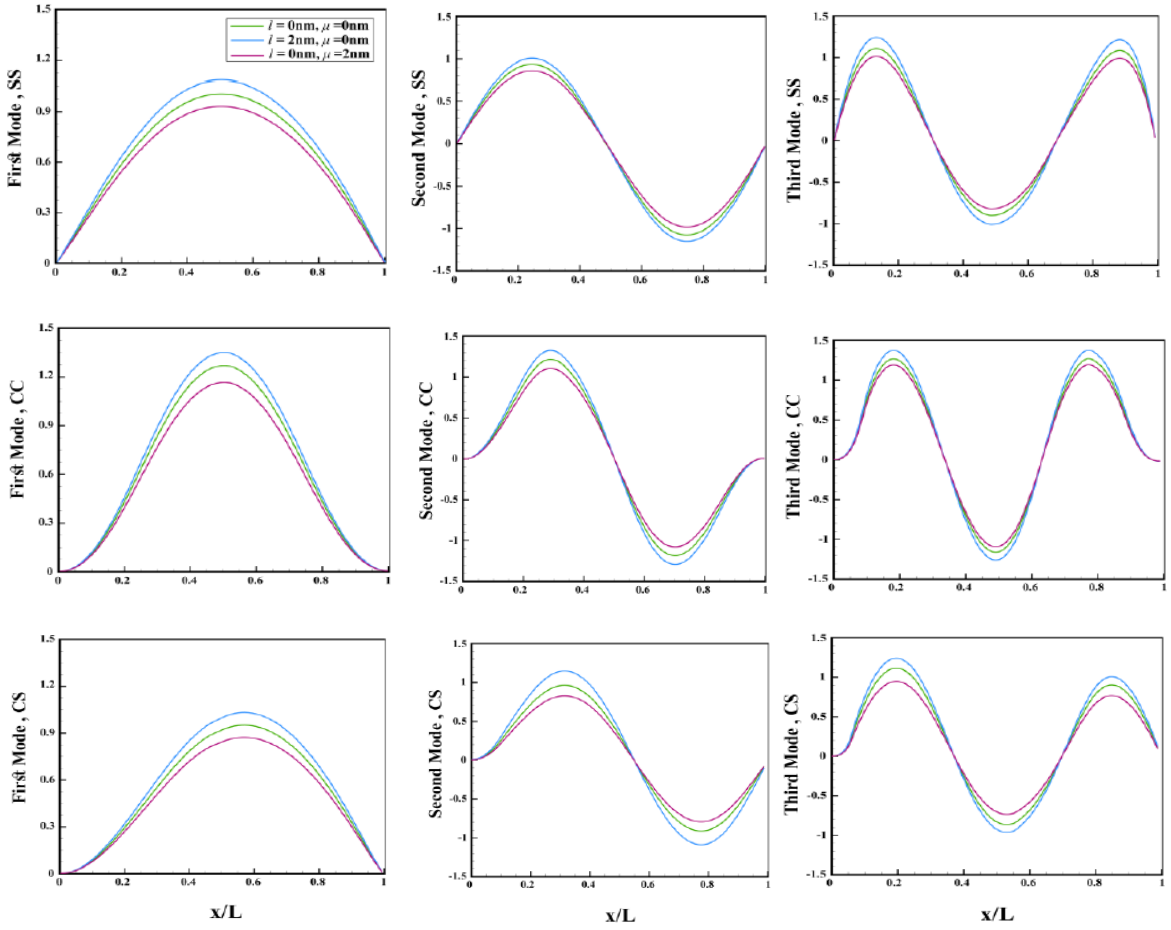

Fig.8

First three mode shapes of CC, SS, and CS BNNT versus x/L .

Finally, the effect of VDW force on the dimensionless frequency with respect to flow velocity is illustrated in Fig. 9 for different boundary conditions. Here, $L/R = 10$, $\Delta T = 0$, $\mu = 0.4\,nm$, $l = 0.3\,nm$, and $V_0 = 0$. It is seen that by considering VDW interaction, the natural frequency increases as VDW forces increase the stiffness of the structure.

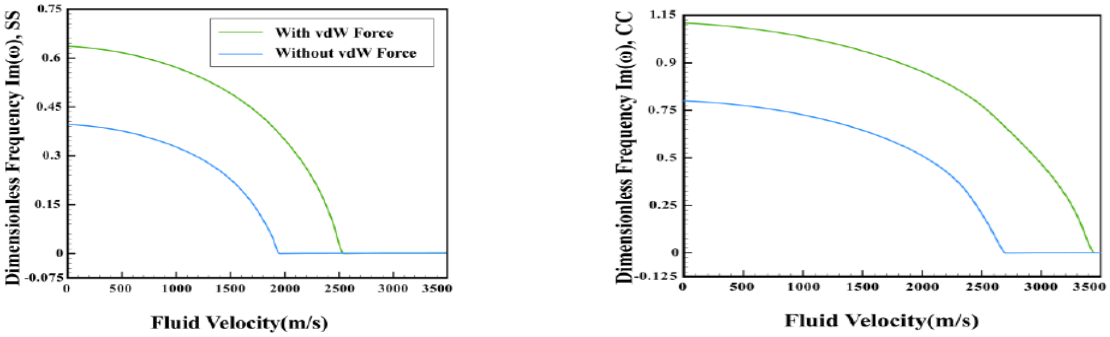

© 2021 IAU, Arak Branch

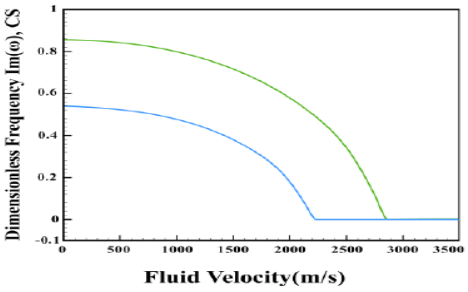

Fig.9
The effect of VDW force on the variation of natural frequency.

5 CONCLUSIONS

A numerical model was presented to investigate the size-dependent free vibration problem of two vertically-aligned SWBNNTs conveying fluid using the nonlocal strain gradient piezoelectric theory in conjunction with the first-order shear deformation shell model. The two adjacent SWBNNTs were coupled with each other by Van Der Waals (VDW) interaction. The governing partial formulations was derived using Hamilton's principle, after which DQM was implemented to solve equilibrium equations. Finally, the numerical results were displayed to denote how the dimensionless complex eigenfrequency is altered by varying the temperature change, aspect ratio, small scale parameters, inter-tube distance, and boundary conditions. The major results are summed up as follows

- The results denoted that VDW force is a significant parameter and cannot be neglected in the analysis.
- By incrementing the nonlocal term, the system frequency and critical flow velocity decrease for all boundary conditions
- By increasing the strain gradient parameter, the critical flow velocity and the natural frequency increase.
- An increase in the value of inter-tube distance brings about a decrease in natural frequency.

APPENDIX A

$$\partial u_i : A_{11}\left(\frac{\partial^2 u_i}{\partial x^2}-l^2\frac{\partial^4 u_i}{\partial x^4}-\frac{l^2}{R^2}\frac{\partial^4 u_1}{\partial x^2\partial\theta^2}\right)+B_{11}\left(\frac{\partial^2\psi_{xi}}{\partial x^2}-l^2\frac{\partial^4\psi_{xi}}{\partial x^4}-\frac{l^2}{R^2}\frac{\partial^4\psi_{xi}}{\partial x^2\partial\theta^2}\right)+$$
$$A_{12}\left[\frac{1}{R}\left(\frac{\partial^2 v_i}{\partial x\,\partial\theta}+\frac{\partial w_i}{\partial x}\right)-\frac{l^2}{R}\left(\frac{\partial^4 v_i}{\partial x^3\partial\theta}+\frac{\partial^3 w_i}{\partial x^3}\right)-\frac{l^2}{R^3}\left(\frac{\partial^4 v_i}{\partial x^3\partial\theta^3}+\frac{\partial^3 w_i}{\partial x\,\partial\theta^2}\right)\right]+\frac{B_{12}}{R}\left(\frac{\partial^2\psi_{\theta i}}{\partial x\,\partial\theta}-\right.$$
$$\left.l^2\frac{\partial^4\psi_{\theta i}}{\partial x^3\partial\theta}-\frac{l^2}{R^2}\frac{\partial^4\psi_{\theta i}}{\partial x\,\partial\theta^3}\right)+F_{31}\left(\frac{\partial\varphi_i}{\partial x}-l^2\frac{\partial^3\varphi_i}{\partial x^3}-\frac{l^2}{R^2}\frac{\partial^3\varphi_i}{\partial x\,\partial\theta^2}\right)+\frac{A_{66}}{R}\left(\frac{\partial^2 v_i}{\partial x\,\partial\theta}+\frac{1}{R}\frac{\partial^2 u_i}{\partial\theta^2}-\right.$$
$$\left.l^2\frac{\partial^4 v_i}{\partial x^3\partial\theta}-\frac{l^2}{R}\frac{\partial^4 u_i}{\partial x^2\partial\theta^2}-\frac{l^2}{R^2}\frac{\partial^4 v_i}{\partial x\,\partial\theta^3}-\frac{l^2}{R^3}\frac{\partial^4 u_i}{\partial\theta^4}\right)+\frac{B_{66}}{R}\left(\frac{\partial^2\psi_{\theta i}}{\partial x\,\partial\theta}+\frac{1}{R}\frac{\partial^2\psi_{xi}}{\partial\theta^2}-l^2\frac{\partial^4\psi_{\theta i}}{\partial x^3\partial\theta}-\right.$$
$$\left.\frac{l^2}{R}\frac{\partial^4\psi_{xi}}{\partial x^2\partial\theta^2}-\frac{l^2}{R^2}\frac{\partial^4\psi_{\theta i}}{\partial x\,\partial\theta^3}-\frac{l^2}{R^3}\frac{\partial^4\psi_{xi}}{\partial\theta^4}\right)=I_0\left(\frac{\partial^2 u_i}{\partial t^2}-\mu^2\frac{\partial^4 u_i}{\partial x^2\partial t^2}-\frac{\mu^2}{R^2}\frac{\partial^4 u_i}{\partial t^2\partial\theta^2}\right)+$$
$$I_1\left(\frac{\partial^2\psi_{xi}}{\partial t^2}-\mu^2\frac{\partial^4\psi_{xi}}{\partial x^2\partial t^2}-\frac{\mu^2}{R^2}\frac{\partial^4\psi_{xi}}{\partial t^2\partial\theta^2}\right),$$
$$\delta v_i : A_{66}\left(\frac{\partial^2 v_i}{\partial x^2}+\frac{1}{R}\frac{\partial^2 u_i}{\partial x\,\partial\theta}-l^2\frac{\partial^4 v_i}{\partial x^4}-\frac{l^2}{R}\frac{\partial^4 u_i}{\partial x^3\partial\theta}-\frac{l^2}{R^2}\frac{\partial^4 v_i}{\partial x^2\partial\theta^2}-\frac{l^2}{R^3}\frac{\partial^4 u_i}{\partial x\,\partial\theta^3}\right)+$$
$$B_{66}\left(\frac{\partial^2\psi_{\theta i}}{\partial x^2}+\frac{l}{R}\frac{\partial^2\psi_{xi}}{\partial x\,\partial\theta}-l^2\frac{\partial^4\psi_{\theta i}}{\partial x^4}-\frac{l^2}{R}\frac{\partial^4\psi_{xi}}{\partial x^3\partial\theta}-\frac{l^2}{R^2}\frac{\partial^4\psi_{\theta i}}{\partial x^2\partial\theta^2}-\frac{l^2}{R^3}\frac{\partial^4\psi_{xi}}{\partial x\,\partial\theta^3}\right)+\frac{A_{12}}{R}\left(\frac{\partial^2 u_i}{\partial x\,\partial\theta}-\right.$$

© 2021 IAU, Arak Branch

$$l^2\frac{\partial^4 u_i}{\partial x^3\partial\theta}-\frac{l^2}{R^2}\frac{\partial^4 u_i}{\partial x\,\partial\theta^3}\Bigg)+\frac{B_{12}}{R}\left(\frac{\partial^2\psi_{xi}}{\partial x\,\partial\theta}-l^2\frac{\partial^4\psi_{xi}}{\partial x^3\partial\theta}-\frac{l^2}{R^2}\frac{\partial^4\psi_{xi}}{\partial x\,\partial\theta^3}\right)+\frac{A_{11}}{R}\Bigg[\frac{1}{R}\left(\frac{\partial^2 v_i}{\partial\theta^2}+\frac{\partial w_i}{\partial\theta}\right)-$$

$$\frac{l^2}{R}\left(\frac{\partial^4 v_i}{\partial x^2\partial\theta^2}+\frac{\partial^3 w_i}{\partial x^2\partial\theta}\right)-\frac{l^2}{R^3}\left(\frac{\partial^4 v_i}{\partial\theta^4}+\frac{\partial^3 w_i}{\partial\theta^3}\right)\Bigg]+\frac{B_{11}}{R}\left(\frac{1}{R}\frac{\partial^2\psi_{\theta i}}{\partial\theta^2}-\frac{l^2}{R}\frac{\partial^2\psi_{\theta i}}{\partial x^2\partial\theta^2}-\frac{l^2}{R^3}\frac{\partial^4\psi_{\theta i}}{\partial\theta^4}\right)+$$

$$F_{31}\left(\frac{\partial\varphi_i}{\partial\theta}-l^2\frac{\partial^3\varphi_i}{\partial x^2\partial\theta}-\frac{l^2}{R^2}\frac{\partial^3\varphi_i}{\partial\theta^3}\right)+\frac{k_s}{R}A_{44}\left(\psi_{\theta i}+\frac{1}{R}\frac{\partial w_i}{\partial\theta}-\frac{v_i}{R}-l^2\frac{\partial^2\psi_{\theta i}}{\partial x^2}-\frac{l^2}{R}\frac{\partial^3 w_i}{\partial x^2\partial\theta}+\right.$$

$$\left.\frac{l^2}{R}\frac{\partial^2 v_i}{\partial x^2}-\frac{l^2}{R^2}\frac{\partial^2\psi_{\theta i}}{\partial\theta^2}-\frac{l^2}{R^3}\frac{\partial^3 w_i}{\partial\theta^3}+\frac{l^2}{R^3}\frac{\partial^2 v_i}{\partial\theta^2}\right)-\frac{k_s}{R}F_{24}\left(\frac{\partial\varphi_i}{\partial\theta}-l^2\frac{\partial^3\varphi_i}{\partial x^2\partial\theta}-\frac{l^2}{R^2}\frac{\partial^3\varphi_i}{\partial\theta^3}\right)-$$

$$\left(N_x^T+N_E\right)\left(\frac{\partial^2 v_i}{\partial x^2}-\mu^2\frac{\partial^4 v_i}{\partial x^4}-\frac{\mu^2}{R^2}\frac{\partial^4 v_i}{\partial x^2\partial\theta^2}\right)+Cy\Bigg[\left(v_i-v_i\right)-\mu^2\left(\frac{\partial^2 v_i}{\partial x^2}-\frac{\partial^2 v_i}{\partial x^2}\right)-$$

$$\frac{\mu^2}{R^2}\left(\frac{\partial^2 v_i}{\partial\theta^2}-\frac{\partial^2 v_i}{\partial\theta^2}\right)\Bigg]=I_0\left(\frac{\partial^2 v_i}{\partial t^2}-\mu^2\frac{\partial^4 v_i}{\partial x^2\partial t^2}-\frac{\mu^2}{R^2}\frac{\partial^4 v_i}{\partial t^2\partial\theta^2}\right)+I_1\left(\frac{\partial^2\psi_{\theta i}}{\partial t^2}-\mu^2\frac{\partial^4\psi_{\theta i}}{\partial x^2\partial t^2}-\frac{\mu^2}{R^2}\frac{\partial^4\psi_{\theta i}}{\partial t^2\partial\theta^2}\right),$$

$$\delta w_i:k_sA_{55}\left(\frac{\partial\psi_{xi}}{\partial x}+\frac{\partial^2 w_i}{\partial x^2}-l^2\frac{\partial^3\psi_{xi}}{\partial x^3}-l^2\frac{\partial^4 w_i}{\partial x^4}-\frac{l^2}{R^2}\frac{\partial^3\psi_{xi}}{\partial x\,\partial\theta^2}-\frac{l^2}{R^2}\frac{\partial^4 w_i}{\partial x^2\partial\theta^2}\right)+$$

$$k_sF_{15}\left(\frac{\partial^2\varphi_i}{\partial x^2}-l^2\frac{\partial^4\varphi_i}{\partial x^4}-\frac{l^2}{RR^2}\frac{\partial^4\varphi_i}{\partial x^2\partial\theta^2}\right)+\frac{k_sA_{44}}{R}\left(\frac{\partial\psi_{\theta i}}{\partial\theta}+\frac{1}{R}\frac{\partial^2 w_i}{\partial\theta^2}-\frac{1}{R}\frac{\partial v_i}{\partial\theta}-l^2\frac{\partial^3\psi_{\theta i}}{\partial x^2\partial\theta}-\right.$$

$$\left.\frac{l^2}{R}\frac{\partial^4 w_i}{\partial x^2\partial\theta^2}+\frac{l^2}{R}\frac{\partial^3 v_i}{\partial x^2\partial\theta}-\frac{l^2}{R^2}\frac{\partial^3\psi_{\theta i}}{\partial\theta^3}-\frac{l^2}{R^3}\frac{\partial^4 w_i}{\partial\theta^4}+\frac{l^2}{R^3}\frac{\partial^3 v_i}{\partial\theta^3}\right)-\frac{k_s}{R}F_{24}\left(\frac{\partial^2\varphi_i}{\partial\theta^2}-l^2\frac{\partial^4\varphi_i}{\partial x^2\partial\theta^2}-\right.$$

$$\left.\frac{l^2}{R^2}\frac{\partial^4\varphi_i}{\partial\theta^4}\right)-\frac{A_{12}}{R}\left(\frac{\partial u_i}{\partial x}-l^2\frac{\partial^3 u_i}{\partial x^3}-\frac{l^2}{R^2}\frac{\partial^3 u_i}{\partial x\,\partial\theta^2}\right)-\frac{B_{12}}{R}\left(\frac{\partial\psi_{xi}}{\partial x}-l^2\frac{\partial^3\psi_{xi}}{\partial x^3}-\frac{l^2}{R^2}\frac{\partial^3\psi_{xi}}{\partial x\,\partial\theta^2}\right)-$$

$$\frac{A_{11}}{R}\left[\frac{1}{R}\left(\frac{\partial v_i}{\partial\theta}+w_i\right)-\frac{l^2}{R}\left(\frac{\partial^3 v_i}{\partial x^2\partial\theta}+\frac{\partial^2 w_i}{\partial x^2}\right)-\frac{l^2}{R^3}\left(\frac{\partial^3 v_i}{\partial\theta^3}+\frac{\partial^3 w_i}{\partial\theta^2}\right)\right]-\frac{B_{11}}{R}\left(\frac{\partial\psi_{\theta i}}{\partial\theta}-l^2\frac{\partial^3\psi_{\theta i}}{\partial x^2\partial\theta}-\right.$$

$$\left.\frac{l^2}{R^2}\frac{\partial^3\psi_{\theta i}}{\partial\theta^3}\right)-\frac{F_{31}}{R}\left(\varphi_i-l^2\frac{\partial^2\varphi_i}{\partial x^2}-\frac{l^2}{R^2}\frac{\partial^2\varphi_i}{\partial\theta^2}\right)-\rho_f\Bigg[\left(\frac{\partial^2 w_i}{\partial t^2}+2U\frac{\partial^2 w_i}{\partial x\,\partial t}+U^2\frac{\partial^2 w_i}{\partial x^2}\right)-$$

$$\mu^2\left(\frac{\partial^4 w_i}{\partial x^2\partial t^2}+2U\frac{\partial^4 w_i}{\partial x^3\partial t}+U^2\frac{\partial^4 w_i}{\partial x^4}\right)-\frac{\mu^2}{R^2}\left(\frac{\partial^4 w_i}{\partial\theta^2\partial t^2}+2U\frac{\partial^4 w_i}{\partial x\,\partial\theta^2\partial t}+U^2\frac{\partial^4 w_i}{\partial x^2\partial\theta^2}\right)\Bigg]-$$

$$\left(N_x^T+N_E\right)\left(\frac{\partial^2 w_i}{\partial x^2}-\mu^2\frac{\partial^4 w_i}{\partial x^4}-\frac{\mu^2}{R^2}\frac{\partial^4 w_i}{\partial t^2\partial\theta^2}\right)+C_z\Bigg[\left(w_i-w_j\right)-\mu^2\left(\frac{\partial^2 w_i}{\partial x^2}-\frac{\partial^2 w_i}{\partial x^2}\right)-$$

$$\frac{\mu^2}{R^2}\left(\frac{\partial^2 w_i}{\partial\theta^2}-\frac{\partial^2 w_j}{\partial\theta^2}\right)\Bigg]=I_0\left(\frac{\partial^2 w_i}{\partial t^2}-\mu^2\frac{\partial^4 w_i}{\partial x^2\partial t^2}-\frac{\mu^2}{R^2}\frac{\partial^4 w_i}{\partial t^2\partial\theta^2}\right),$$

$$\delta\psi_{xi}:B_{11}\left(\frac{\partial^2 u_i}{\partial x^2}-l^2\frac{\partial^4 u_i}{\partial x^4}-\frac{l^2}{R^2}\frac{\partial^4 u_i}{\partial x^2\partial\theta^2}\right)+D_{11}\left(\frac{\partial^2\psi_{xi}}{\partial x^2}-l^2\frac{\partial^4\psi_{xi}}{\partial x^4}-\frac{l^2}{R^2}\frac{\partial^4\psi_{xi}}{\partial x^2\partial\theta^2}\right)+$$

$$B_{12}\left[\frac{1}{R}\left(\frac{\partial^2 v_i}{\partial x\,\partial\theta}+\frac{\partial w_i}{\partial x}\right)-\frac{l^2}{R}\left(\frac{\partial^4 v_i}{\partial x^3\partial\theta}+\frac{\partial^3 w_i}{\partial x^3}\right)-\frac{l^2}{R^3}\left(\frac{\partial^4 v_i}{\partial x\,\partial\theta^3}+\frac{\partial^3 w_i}{\partial x\,\partial\theta^2}\right)\right]+\frac{D_{12}}{R}\left(\frac{\partial^2\psi_{\theta i}}{\partial x\,\partial\theta}-\right.$$

© 2021 IAU, Arak Branch

$$l^2\frac{\partial^4\psi_{\theta i}}{\partial x^3\partial\theta}-\frac{l^2}{R^2}\frac{\partial^4\psi_{\theta i}}{\partial x\,\partial\theta^3}\Bigg)+G_{31}\left(\frac{\partial\varphi_i}{\partial x}-l^2\frac{\partial^3\varphi_i}{\partial x^3}-\frac{l^2}{R^2}\frac{\partial^3\varphi_i}{\partial x\,\partial\theta^2}\right)+\frac{B_{66}}{R}\left(\frac{\partial^2 v_i}{\partial x\,\partial\theta}+\frac{1}{R}\frac{\partial^2 u_i}{\partial\theta^2}-\right.$$

$$l^2\frac{\partial^4 v_i}{\partial x^3\partial\theta}-\frac{l^2}{R}\frac{\partial^4 u_i}{\partial x^2\partial\theta^2}-\frac{l^2}{R^2}\frac{\partial^4 v_i}{\partial x\,\partial\theta^3}-\frac{l^2}{R^3}\frac{\partial^4 u_i}{\partial\theta^4}\Bigg)+\frac{D_{66}}{R}\left(\frac{\partial^2\psi_{\theta i}}{\partial x\,\partial\theta}+\frac{1}{R}\frac{\partial^2\psi_{xi}}{\partial\theta^2}-l^2\frac{\partial^4\psi_{\theta i}}{\partial x^3\partial\theta}-\right.$$

$$\frac{l^2}{R}\frac{\partial^4\psi_{xi}}{\partial x^2\partial\theta^2}-\frac{l^2}{R^2}\frac{\partial^4\psi_{\theta i}}{\partial x\,\partial\theta^3}-\frac{l^2}{R^3}\frac{\partial^4\psi_{xi}}{\partial\theta^4}-\Bigg)-k_sA_{55}\left[\left(\psi_{xi}+\frac{\partial w_i}{\partial x}\right)-l^2\left(\frac{\partial^2\psi_{xi}}{\partial x^2}+\frac{\partial^3 w_i}{\partial x^3}\right)-\right.$$

$$\left.\frac{l^2}{R^2}\left(\frac{\partial^2\psi_{xi}}{\partial\theta^2}+\frac{\partial^3 w_i}{\partial x\,\partial\theta^2}\right)\right]+k_sF_{15}\left(\frac{\partial\varphi_i}{\partial x}-l^2\frac{\partial^3\varphi_i}{\partial x^3}-\frac{l^2}{R^2}\frac{\partial^3\varphi_i}{\partial x\,\partial\theta^2}\right)=I_1\left(\frac{\partial^2 u_i}{\partial t^2}-\mu^2\frac{\partial^4 u_i}{\partial x^2\partial t^2}-\right.$$

$$\left.\frac{\mu^2}{R^2}\frac{\partial^4 u_i}{\partial t^2\partial\theta^2}\right)+I_2\left(\frac{\partial^2\psi_{xi}}{\partial t^2}-\mu^2\frac{\partial^4\psi_{xi}}{\partial x^2\partial t^2}-\frac{\mu^2}{R^2}\frac{\partial^4\psi_{xi}}{\partial t^2\partial\theta^2}\right),$$

$$\psi_{\theta i}:B_{66}\left(\frac{\partial^2 v_i}{\partial x^2}+\frac{1}{R}\frac{\partial^2 u_i}{\partial x\,\partial\theta}-l^2\frac{\partial^4 v_i}{\partial x^4}-\frac{l^2}{R}\frac{\partial^4 u_i}{\partial x^3\partial\theta}-\frac{l^2}{R^2}\frac{\partial^4 v_i}{\partial x^2\partial\theta^2}-\frac{l^2}{R^3}\frac{\partial^4 u_i}{\partial x\,\partial\theta^3}\right)+$$

$$D_{66}\left(\frac{\partial^2\psi_{xi}}{\partial x^2}+\frac{1}{R}\frac{\partial^2\psi_{xi}}{\partial x\,\partial\theta}-l^2\frac{\partial^4\psi_{xi}}{\partial x^4}-\frac{l^2}{R}\frac{\partial^4\psi_{xi}}{\partial x^3\partial\theta}-\frac{l^2}{R^2}\frac{\partial^4\psi_{xi}}{\partial x^2\partial\theta^2}-\frac{l^2}{R^3}\frac{\partial^4\psi_{xi}}{\partial x\,\partial\theta^3}\right)+\frac{B_{12}}{R}\left(\frac{\partial^2 u_i}{\partial x\,\partial\theta}-\right.$$

$$l^2\frac{\partial^4 u_i}{\partial x^3\partial\theta}-\frac{l^2}{R^2}\frac{\partial^4 u_i}{\partial x\,\partial\theta^3}\Bigg)+\frac{D_{12}}{R}\left(\frac{\partial^2\psi_{xi}}{\partial x\,\partial\theta}-l^2\frac{\partial^4\psi_{xi}}{\partial x^3\partial\theta}-\frac{l^2}{R^2}\frac{\partial^4\psi_{xi}}{\partial x\,\partial\theta^3}\right)+\frac{B_{11}}{R}\left[\frac{1}{R}\left(\frac{\partial^2 v_i}{\partial\theta^2}+\frac{\partial w_i}{\partial\theta}\right)-\right.$$

$$\left.\frac{l^2}{R}\left(\frac{\partial^4 v_i}{\partial x^2\partial\theta^2}+\frac{\partial^3 w_i}{\partial x^2\partial\theta}\right)-\frac{l^2}{R^3}\left(\frac{\partial^4 v_i}{\partial\theta^4}+\frac{\partial^3 w_i}{\partial\theta^3}\right)\right]+\frac{D_{11}}{R}\left(\frac{1}{R}\frac{\partial^2\psi_{\theta i}}{\partial\theta^2}-\frac{l^2}{R}\frac{\partial^4\psi_{\theta i}}{\partial x^2\partial\theta^2}-\frac{l^2}{R^3}\frac{\partial^4\psi_{\theta i}}{\partial\theta^4}\right)+$$

$$G_{31}\left(\frac{\partial\varphi_i}{\partial\theta}-l^2\frac{\partial^3\varphi_i}{\partial x^2\partial\theta}-\frac{l^2}{R^2}\frac{\partial^3\varphi_i}{\partial\theta^3}\right)-k_sA_{44}\left(\psi_{\theta i}+\frac{1}{R}\frac{\partial w_i}{\partial\theta}-\frac{v_i}{R}-l^2\frac{\partial^2\psi_{\theta i}}{\partial x^2}-\frac{l^2}{R}\frac{\partial^3 w_i}{\partial x^2\partial\theta}+\right.$$

$$\frac{l^2}{R}\frac{\partial^2 v_i}{\partial x^2}-\frac{l^2}{R^2}\frac{\partial^2\psi_{\theta i}}{\partial\theta^2}-\frac{l^2}{R^3}\frac{\partial^3 w_i}{\partial\theta^3}+\frac{l^2}{R^3}\frac{\partial^2 v_i}{\partial\theta^2}\Bigg)+k_sF_{24}\left(\frac{\partial\varphi_i}{\partial\theta}-l^2\frac{\partial^3\varphi_i}{\partial x^2\partial\theta}-\frac{l^2}{R^2}\frac{\partial^3\varphi_i}{\partial\theta^3}\right)=$$

$$I_1\left(\frac{\partial^2 v_i}{\partial t^2}-\mu^2\frac{\partial^4 v_i}{\partial x^2\partial t^2}-\frac{\mu^2}{R^2}\frac{\partial^4 v_i}{\partial t^2\partial\theta^2}\right)+I_2\left(\frac{\partial^2\psi_{\theta i}}{\partial t^2}-\mu^2\frac{\partial^4\psi_{\theta i}}{\partial x^2\partial t^2}-\frac{\mu^2}{R^2}\frac{\partial^4\psi_{\theta i}}{\partial t^2\partial\theta^2}\right),$$

$$\delta\varphi_i:F_{15}\left[\left(\frac{\partial\psi_{xi}}{\partial x}+\frac{\partial^2 w_i}{\partial x^2}\right)-l^2\left(\frac{\partial^3\psi_{xi}}{\partial x^3}+\frac{\partial^4 w_i}{\partial x^4}\right)-\frac{l^2}{R^2}\left(\frac{\partial^3\psi_{xi}}{\partial x\,\partial\theta^2}+\frac{\partial^4 w_i}{\partial x^2\partial\theta^2}\right)\right]+$$

$$P_{11}\left(\frac{\partial^2\varphi_i}{\partial x^2}-l^2\frac{\partial^4\varphi_i}{\partial x^4}-\frac{l^2}{R^2}\frac{\partial^4\varphi_i}{\partial x^2\partial\theta^2}\right)+F_{24}\left[\frac{\partial\psi_{\theta i}}{\partial\theta}+\frac{1}{R}\frac{\partial^2 w_i}{\partial\theta^2}-\frac{\partial v_i}{R\,\partial\theta}-l^2\left(\frac{\partial^3\psi_{\theta i}}{\partial x^2\partial\theta}+\right.\right.$$

$$\left.\frac{1}{R}\frac{\partial^4 w_i}{\partial x^2\partial\theta^2}-\frac{\partial^4 u_i}{R\,\partial x^2\partial\theta}\right)-\frac{l^2}{R^2}\left(\frac{\partial^3\psi_{\theta i}}{\partial\theta^3}+\frac{1}{R}\frac{\partial^4 w_i}{\partial\theta^4}-\frac{\partial^3 v_i}{R\,\partial\theta^3}\right)\Bigg]+P_{22}\left(\frac{\partial^2\varphi_i}{\partial\theta^2}-l^2\frac{\partial^4\varphi_i}{\partial x^2\partial\theta^2}-\right.$$

$$\left.\frac{l^2}{R^2}\frac{\partial^4\varphi_i}{\partial\theta^4}\right)+F_{31}\left(\frac{\partial u_i}{\partial x}-l^2\frac{\partial^3 u_i}{\partial x^3}-\frac{l^2}{R^1}\frac{\partial^3 u_i}{\partial x\,\partial\theta^2}\right)+G_{31}\left(\frac{\partial\psi_{xi}}{\partial x}-l^2\frac{\partial^3\psi_{xi}}{\partial x^3}-\frac{l^2}{R^2}\frac{\partial^3\psi_{xi}}{\partial x\,\partial\theta^2}\right)+$$

© 2021 IAU, Arak Branch

$$F_{31}\left[\frac{1}{R}\left(\frac{\partial v_i}{\partial\theta}+\partial^2 w_i\right)-\frac{l^2}{R}\left(\frac{\partial^3 v_i}{\partial x^2\partial\theta}+\frac{\partial^2 w_i}{\partial x^2}\right)-\frac{l^2}{R^3}\left(\frac{\partial^3 v_i}{\partial\theta^3}+\frac{\partial^3 w_i}{\partial\theta^2}\right)\right]+\frac{G_{31}}{R}\left(\frac{\partial\psi_{\theta i}}{\partial\theta}-l^2\frac{\partial^3\psi_{\theta i}}{\partial x^2\partial\theta}-\right.$$
$$\left.\frac{l^2}{R^2}\frac{\partial^3\psi_{\theta i}}{\partial\theta^3}\right)-P_{33}\left(\varphi_i-l^2\frac{\partial^2\varphi_i}{\partial x^2}-\frac{l^2}{R^2}\frac{\partial^2\varphi_i}{\partial\theta^2}\right)=0$$

In which $\mu=(e_0 a)$ and

$$\langle A_{11},A_{12}\rangle=\int_{-\frac{h}{2}}^{\frac{h}{2}}\frac{E}{1-\vartheta^2}\langle 1-\vartheta\rangle dz\,,\ \langle B_{11},B_{12}\rangle=\int_{-\frac{h}{2}}^{\frac{h}{2}}\frac{E}{1-\vartheta^2}\langle 1-\vartheta\rangle z dz\,,$$

$$\langle D_{11},D_{12}\rangle=\int_{-\frac{h}{2}}^{\frac{h}{2}}\frac{E}{1-\vartheta^2}\langle 1-\vartheta\rangle z^2 dz\,,A_{66}=A_{55}=A_{44}=\int_{-\frac{h}{2}}^{\frac{h}{2}}\frac{E}{2(1+\vartheta)}dz\,,$$

$$\langle B_{66},B_{66}\rangle=\int_{-\frac{h}{2}}^{\frac{h}{2}}\frac{E}{2(1+\vartheta)}\langle 1,z\rangle z dz\,,\langle F_{31},G_{31}\rangle=\int_{-\frac{h_1}{2}}^{\frac{h_1}{2}}e_{31}\left(\frac{\pi}{h_1}\right)\sin\left(\frac{\pi z}{h_1}\right)\langle 1,z\rangle dz\,,$$

$$F_{24}=\int_{-\frac{h_1}{2}}^{\frac{h_1}{2}}\frac{e_{24}}{z+R_1}\cos\left(\frac{\pi z}{h_1}\right)dz\,,\ F_{15}=\int_{-\frac{h_1}{2}}^{\frac{h_1}{2}}e_{24}\cos\left(\frac{\pi z}{h_1}\right)dz\,,$$

$$P_{11}=\int_{-\frac{h_1}{2}}^{\frac{h_1}{2}}s_{11}\cos^2\left(\frac{\pi z}{h_1}\right)dz\,,\ P_{22}=\int_{-\frac{h_1}{2}}^{\frac{h_1}{2}}\frac{s_{22}}{z+R_1}\cos^2\left(\frac{\pi z}{h_1}\right)dz\,,$$

$$P_{33}=\int_{-\frac{h_1}{2}}^{\frac{h_1}{2}}s_{33}\left(\frac{\pi}{h_1}\right)^2\sin^2\left(\frac{\pi z}{h_1}\right)dz$$

REFERENCES

[1] Lieber C.M., 1998, One-dimensional nanostructures: chemistry, physics & applications, *Solid State Commun* **107**: 607-616.

[2] Dresselhaus M.S., Dresselhaus G., Eklund P.C., Rao A.M., 2000, *Carbon Nanotubes, The Physics of Fullerene-Based and Fullerene-Related Materials*, Springer.

[3] Dresselhaus G., Riichiro S., 1998, *Physical Properties of Carbon Nanotubes*, World Scientific.

[4] Zhi C., Bando Y., Tang C., Golberg D., 2010, Boron nitride nanotubes, *Materials Science and Engineering R: Reports* **70**: 92-111.

[5] Pakdel A., Zhi C., Bando Y., Golberg D., 2012, Low-dimensional boron nitride nanomaterials, *Materials Today* **15**: 256-265.

[6] Chopra N.G., Luyken R.J., Cherrey K., 1995, Boron nitride nanotubes, *Science* **269**: 966-967.

[7] Salehi-Khojin A., Jalili N., 2008, Buckling of boron nitride nanotube reinforced piezoelectric polymeric composites subject to combined electro-thermo-mechanical loadings, *Composites Science and Technology* **68**:1489-1501.

[8] Chowdhury R., Wang C.Y., Adhikari S., Scarpa F., 2010, Vibration and symmetry-breaking of boron nitride nanotubes, *Nanotechnology* **21**: 365702.

[9] Ebrahimi-Nejad S., Shokuhfar A., Zare-Shahabadi A., 2010, Molecular dynamics simulation of the buckling behavior of boron nitride nanotubes under uniaxial compressive loading, *Defect and Diffusion Forum* **297-301**: 984-989.

[10] Yang J.H., Yang J., Kitipornchai S., 2012, Nonlinear dynamic response of electro-thermo-mechanically loaded piezoelectric cylindrical shell reinforced with BNNTs, *Smart Materials* and *Structures* **21**: 125005.

[11] Ansari R., Rouhi S., Mirnezhad M., Aryayi M., 2015, Stability characteristics of single-walled boron nitride nanotubes, *Archives of Civil and Mechanical Engineering* **15**: 162-170.

© 2021 IAU, Arak Branch

[12] Yan J.W., He J.B., Tong L.H., 2019, Longitudinal and torsional vibration characteristics of boron nitride nanotubes, *Journal of Vibration Engineering Technologies* **7**: 205-215.
[13] Chen C.Q., Shi Y., Zhang Y.S., 2006, Size dependence of Young's modulus in ZnO nanowires, *Physical Review Letters* **96**: 075505.
[14] Stan G., Ciobanu C.V., Parthangal P.M., Cook R.F., 2007, Diameter-dependent radial and tangential elastic moduli of ZnO nanowires, *Nano Letters* **7**: 3691-3697.
[15] Mindlin R.D., 1964, Micro-structure in linear elasticity, *Archive for Rational Mechanics and Analysis* **16**: 51-78.
[16] Mindlin R.D., Eshel N.N., 1968, On first strain-gradient theories in linear elasticity, *International Journal of Solids and Structures* **4**:109-124.
[17] Mindlin R.D., 1965, Second gradient of strain and surface-tension in linear elasticity, *International Journal of Solids and Structures* **1**: 417-438.
[18] Mindlin R.D., Tiersten H.F., 1962, Effects of couple-stresses in linear elasticity, *Archive for Rational Mechanics and Analysis* **11**: 415-448.
[19] Toupin R.A., 1962, Elastic materials with couple-stresses, *Archive for Rational Mechanics and Analysis* **11**: 385-414.
[20] Eringen A.C., 1972, Linear theory of nonlocal elasticity and dispersion of plane waves, *International Journal of Engineering Science* **10**: 425-435.
[21] Eringen A.C., 1983, On differential equations of nonlocal elasticity and solutions of screw dislocation and surface waves, *Journal of Applied Physics* **54**: 4703-4710.
[22] Lam D.C.C., Yang F., Chong A.C.M., 2003, Experiments and theory in strain gradient elasticity, *Journal of the Mechanics and Physics of Solids* **51**: 1477-1508.
[23] Yang F., Chong A.C.M., Lam D.C.C., Tong P., 2002, Couple stress based strain gradient theory for elasticity, *International Journal of Solids and Structures* **39**: 2731-2743.
[24] Sedighi H.M., Malikan M., 2020, Stress-driven nonlocal elasticity for nonlinear vibration characteristics of carbon/boron-nitride hetero-nanotube subject to magneto-thermal environment, *Physica Scripta* **95**: 55218.
[25] Simsek M., 2011, Forced vibration of an embedded single-walled carbon nanotube traversed by a moving load using nonlocal Timoshenko beam theory, *Steel & Composite Structures* **11**: 59-76.
[26] Arani A.G., Bidgoli A.H., Ravandi A.K., 2013, Induced nonlocal electric wave propagation of boron nitride nanotubes, *Journal of Mechanical Science and Technology* **27**: 3063-3071.
[27] Ghorbanpour Arani A., Jalilvand A., Ghaffari M., 2014, Nonlinear pull-in instability of boron nitride nano-switches considering electrostatic and Casimir forces, *Scientiairanica* **21**: 1183-1196.
[28] Ghorbanpour Arani A., Karamali R.A., Roudbari M.A., 2015, Axial and transverse vibration of SWBNNT system coupled Pasternak foundation under a moving nanoparticle using Timoshenko beam theory, *Journal of Solid Mechanics* **7**: 239-254.
[29] Arani A.G., Roudbari M.A., Amir S., 2016, Longitudinal magnetic field effect on wave propagation of fluid-conveyed SWCNT using Knudsen number and surface considerations, *Applied Mathematical Modelling* **40**: 2025-2038.
[30] Arani A.G., Roudbari M.A., Amir S., 2012, Nonlocal vibration of SWBNNT embedded in bundle of CNTs under a moving nanoparticle, *Physica B Condensed Matter* **407**: 3646–3653.
[31] Ghorbanpour Arani A., Roudbari M.A., Kiani K., 2016, Vibration of double-walled carbon nanotubes coupled by temperature-dependent medium under a moving nanoparticle with multi physical fields, *Mechanics of Advanced Materials and Structures* **23**: 281-291.
[32] Arani A.G., Roudbari M.A., 2014, Surface stress, initial stress and Knudsen-dependent flow velocity effects on the electro-thermo nonlocal wave propagation of SWBNNTs, *Physica B Condensed Matter* **452**: 159-165.
[33] Jorshari T.D., Roudbari M.A., Scerrato D., Kouzani A., 2019, Vibration suppression of a boron nitride nanotube under a moving nanoparticle using a classical optimal control procedure, *Continuum Mechanics and Thermodynamics* **31**: 1825-1842.
[34] Roudbari M.A., Ansari R., 2018, Single-walled boron nitride nanotube as nano-sensor, *Continuum Mechanics and Thermodynamics* **32**: 729-748.
[35] Roudbari M.A., Jorshari T.D., 2018, Vibrational control scrutiny of physically affected SWCNT acted upon by a moving nanoparticle in the framework of nonlocal–strain gradient theory, *Journal of the Brazilian Society of Mechanical Sciences and Engineering* **40**: 499.
[36] Bahaadini R., Saidi A.R., Hosseini M., 2018, Dynamic stability of fluid-conveying thin-walled rotating pipes reinforced with functionally graded carbon nanotubes, *Acta Mechanica* **229**: 5013-5029.
[37] Azarboni H.R., 2019, Magneto-thermal primary frequency response analysis of carbon nanotube considering surface effect under different boundary conditions, *Composites Part B: Engineering* **165**: 435-441.
[38] Tyagi M., Khan A., Husain M., Husain S., 2019, Analytical and computational studies of the nonlinear vibrations of SWCNTs embedded in viscous elastic matrix using KBM method, *Chaos: An Interdisciplinary Journal of Nonlinear Science* **29**: 23134.
[39] Mohammadimehr M., Mohandes M., Moradi M., 2016, Size dependent effect on the buckling and vibration analysis of double-bonded nanocomposite piezoelectric plate reinforced by boron nitride nanotube based on modified couple stress theory, *Journal of Vibration and Control* **22**: 1790-1807.
[40] Mohammadimehr M., Atifeh S.J., Rousta Navi B., 2018, Stress and free vibration analysis of piezoelectric hollow circular FG-SWBNNTs reinforced nanocomposite plate based on modified couple stress theory subjected to thermo-

© 2021 IAU, Arak Branch

mechanical loadings, *Journal of Vibration and Control* **24**: 3471-3486.
[41] Ghorbanpour Arani A., Jalilvand A., Kolahchi R., 2014, Nonlinear strain gradient theory based vibration and instability of boron nitride micro-tubes conveying ferrofluid, *International Applied Mechanics* **6**: 1450060.
[42] Bahaadini R., Hosseini M., Jamalpoor A., 2017, Nonlocal and surface effects on the flutter instability of cantilevered nanotubes conveying fluid subjected to follower forces, *Physica B Condensed Matter* **509**: 55-61.
[43] Saffari P.R., Fakhraie M., Roudbari M.A., 2020, Nonlinear vibration of fluid conveying cantilever nanotube resting on visco-pasternak foundation using non-local strain gradient theory, *Micro & Nano Letters* **15**:181-186.
[44] Arani A.G., Roudbari M.A., 2013, Nonlocal piezoelastic surface effect on the vibration of visco-Pasternak coupled boron nitride nanotube system under a moving nanoparticle, *Thin Solid Films* **542**: 232-241.
[45] Mercan K., Civalek Ö., 2016, DSC method for buckling analysis of boron nitride nanotube (BNNT) surrounded by an elastic matrix, *Composite Structures* **143**: 300-309.
[46] Akgöz B., Civalek Ö., 2016, Bending analysis of embedded carbon nanotubes resting on an elastic foundation using strain gradient theory, *Acta Astronautica* **119**: 1-12.
[47] Lim C.W., Zhang G., Reddy J.N., 2015, A higher-order nonlocal elasticity and strain gradient theory and its applications in wave propagation, *Journal of the Mechanics and Physics of Solids* **78**: 298-313.
[48] Li L., Hu Y., Ling L., 2015, Flexural wave propagation in small-scaled functionally graded beams via a nonlocal strain gradient theory, *Composite Structures* **133**: 1079-1092.
[49] Li L., Hu Y., Ling L., 2016, Wave propagation in viscoelastic single-walled carbon nanotubes with surface effect under magnetic field based on nonlocal strain gradient theory, *Physica E: Low-Dimensional Systems and Nanostructures* **75**: 118-124.
[50] Malikan M., Nguyen V.B., Tornabene F., 2018, Damped forced vibration analysis of single-walled carbon nanotubes resting on viscoelastic foundation in thermal environment using nonlocal strain gradient theory, *Engineering Science and Technology, an International Journal* **21**: 778-786.
[51] Dehghan M., Ebrahimi F., Vinyas M., 2019, Wave dispersion analysis of magnetic-electrically affected fluid-conveying nanotubes in thermal environment, *Proceedings of the Institution of Mechanical Engineers, Part C: Journal of Mechanical Engineering Science*.
[52] Mohammadian M., Hosseini S.M., Abolbashari M.H., 2019, Lateral vibrations of embedded hetero-junction carbon nanotubes based on the nonlocal strain gradient theory: Analytical and differential quadrature element (DQE) methods, *Physica E: Low-Dimensional Systems and Nanostructures* **105**: 68-82.
[53] Arani A.G., Haghparast E., Maraghi Z.K., Amir S., 2015, Nonlocal vibration and instability analysis of embedded DWCNT conveying fluid under magnetic field with slip conditions consideration, *Proceedings of the Institution of Mechanical Engineers, Part C: Journal of Mechanical Engineering Science* **229**: 349-363.
[54] Natsuki T., Ni Q-Q., Endo M., 2009, Analysis of the vibration characteristics of fluid-conveying double-walled carbon nanotubes, *Journal of Applied Physics* **105**: 094328.
[55] Oveissi S., Eftekhari S.A., Toghraie D., 2016, Longitudinal vibration and instabilities of carbon nanotubes conveying fluid considering size effects of nanoflow and nanostructure, *Physica E: Low-Dimensional Systems and Nanostructures* **83**: 164-173.
[56] Cheng Q., Liu Y., Wang G., 2019, Free vibration of a fluid-conveying nanotube constructed by carbon nanotube and boron nitride nanotube, *Physica E: Low-Dimensional Systems and Nanostructures* **109**: 183-190.
[57] Arani A.G., Amir S., 2013, Electro-thermal vibration of visco-elastically coupled BNNT systems conveying fluid embedded on elastic foundation via strain gradient theory, *Physica B Condensed Matter* **419**: 1-6.
[58] Ansari R., Norouzzadeh A., Gholami R., 2014, Size-dependent nonlinear vibration and instability of embedded fluid-conveying SWBNNTs in thermal environment, *Physica E: Low-Dimensional Systems and Nanostructures* **61**: 148-157.
[59] Mahinzare M., Mohammadi K., Ghadiri M., 2019, A nonlocal strain gradient theory for vibration and flutter instability analysis in rotary SWCNT with conveying viscous fluid, *Waves in Random and Complex Media* **31**: 305-330.
[60] Ghorbanpour Arani A.H., Rastgoo A., Hafizi Bidgoli A., 2017, Wave propagation of coupled double-DWBNNTs conveying fluid-systems using different nonlocal surface piezoelasticity theories, *Mechanics of Advanced Materials and Structures* **24**: 1159-1179.
[61] Zeighampour H., Beni Y.T., Karimipour I., 2017, Wave propagation in double-walled carbon nanotube conveying fluid considering slip boundary condition and shell model based on nonlocal strain gradient theory, *Microfluid Nanofluidics* **21**: 85.
[62] Mohammadi K., Rajabpour A., Ghadiri M., 2018, Calibration of nonlocal strain gradient shell model for vibration analysis of a CNT conveying viscous fluid using molecular dynamics simulation, *Computational Materials Science* **148**: 104-115.
[63] Mahinzare M., Mohammadi K., Ghadiri M., Rajabpour A., 2017, Size-dependent effects on critical flow velocity of a SWCNT conveying viscous fluid based on nonlocal strain gradient cylindrical shell model, *Microfluid Nanofluidics* **21**: 123.
[64] Roodgar Saffar P., Fakhraie M., Roudbari M.A., 2020, Free vibration problem of fluid-conveying double-walled boron nitride nanotubes via nonlocal strain gradient theory in thermal environment , *Mechanics Based Design of Structures and Mechanies* **2020**: 1-18.
[65] Zarabimanesh Y., Roodgar Saffari P., Roudgar Saffari P., Refahati N., 2021, Hygro-thermo-mechanical vibration of two vertically aligned single-walled boron nitride nanotubes conveying fluid, *Journal of Vibration and Control*

© 2021 IAU, Arak Branch

doi.org/10.1177/10775463211006512.

[66] Roodgar Saffari P., Fakhraie M., Roudbari M.A, 2020, Free vibration and transient response of heterogeneous piezoelectric sandwich annular plate using third-order shear deformation assumption, *Journal of Solid Mechanics* **12**: 315-333.

[67] Ke L.L., Wang Y.S., Reddy J.N., 2014, Thermo-electro-mechanical vibration of size-dependent piezoelectric cylindrical nanoshells under various boundary conditions, *Composite Structures* **116**: 626-636.

[68] Roodgar Saffari P., Fakhraie M., Roudbari M.A., 2020, Free vibration and transient response of heterogeneous piezoelectric sandwich annular plate using third-order shear deformation assumption, *Journal of Solid Mechanics* **12**: 315-333.

[69] Kiani K., 2014, In-and out-of-plane dynamic flexural behaviors of two-dimensional ensembles of vertically aligned single-walled carbon nanotubes, *Physica B Condensed Matter* **449**: 164-180.

[70] Roudbari M.A., Jorshari T.D., Arani A.G., 2020, Transient responses of two mutually interacting single-walled boron nitride nanotubes induced by a moving nanoparticle, *European Journal* of Mechanics **82**: 103978.

[71] Murmu T., Pradhan S.C., 2010, Thermal effects on the stability of embedded carbon nanotubes, *Computational Materials Science* **47**: 721-726.

[72] Mehralian F., Beni Y.T., 2018, Vibration analysis of size-dependent bimorph functionally graded piezoelectric cylindrical shell based on nonlocal strain gradient theory, *Journal of the Brazilian Society of Mechanical Sciences and Engineering* **40**: 27.

[73] Ke L-L., Wang Y-S., 2011, Flow-induced vibration and instability of embedded double-walled carbon nanotubes based on a modified couple stress theory, *Physica E: Low-Dimensional Systems and Nanostructures* **43**: 1031-1039.

© 2021 IAU, Arak Branch